Research Article

Small-molecule degraders reduce Aβ production through CAPRIN1-mediated lysosomal degradation of APP in Alzheimer's iPSC-derived neurons

Sunghan Jung,[1] Nancy Jaiswal,[1] Ratan K. Rai[2], Yuichiro Takagi,[2] Ho-Yin Lo,[3] Cen Gao,[1] Lifan Zeng,[2] Xu Wang,[1] Reagan K. Wohlford,[1] Ryan K. Higgins,[1] Anita C. Bellail,[1] Chunhai Hao[1,4]

[1]Department of Pathology and Laboratory Medicine, Indiana University School of Medicine, Indianapolis, Indiana, USA

[2]Department of Biochemistry and Molecular Biology, Indiana University School of Medicine, Indianapolis, Indiana, USA

[3]Synovel Laboratory LLC, Danbury, Connecticut, USA

[4]Stark Neurosciences Research Institute, Indiana University School of Medicine, Indianapolis, Indiana, USA.

Correspondence

Chunhai Hao, Department of Pathology and Laboratory Medicine, Indiana University School of Medicine, Indianapolis, IN 46202, USA.

Email: chunhao@iu.edu

Anita C. Bellail, Department of Pathology and Laboratory Medicine, Indiana University School of Medicine, Indianapolis, IN 46202, USA.

Email: abellail@iu.edu

Funding Information

Indiana University School of Medicine Physician Scientist Initiative funded by Lilly Endowment, Inc., research fund from the Department of Pathology & Laboratory Medicine and the Endowment fund of the Bicentennial Chair of the Indiana University School of Medicine to Chunhai Hao.

Abstract

INTRODUCTION: The amyloid cascade of amyloid β (Aβ) production from amyloid precursor protein (APP) plays a key role in the pathogenesis of Alzheimer's disease (AD). However, disease-modifying therapies to disrupt this amyloid cascade remain an unmet challenge.

METHODS: Using neurons and organoids differentiated from induced pluripotent stem cells (iPSCs) derived from sporadic and familiar AD patients, we identified small-molecule degraders that reduce Aβ through screening of our library of cytoplasmic activation/proliferation-associate protein 1 (CAPRIN1)-targeted small-molecules.

RESULTS: The small-molecule degraders act as molecular glues that bind CAPRIN1 and APP and enhance the protein-protein interaction. Tracking CAPRIN1 and APP in neurons revealed that the degraders induce CAPRIN1-mediated APP degradation through the endosomal-lysosomal pathway and thus reduce Aβ peptide production in AD iPSC neurons and extracellular deposition in AD iPSC organoids.

DISCUSSION: The small-molecule degraders provide new therapeutics through targeted protein degradation of APP and disruption of the amyloid cascade in AD brain.

KEYWORKDS

Alzheimer's disease, amyloid β, amyloid precursor protein, cytoplasmic activation/proliferation-associate protein 1, induced pluripotent stem cell, lysosome, molecular glue, small-molecule degrader, targeted protein degradation

HIGHTLIGHTS

- Here, we report the discovery of small-molecule degrader compounds that degrade APP and reduce Aβ peptide production.
- The APP degrader compounds act as molecular glues that directly bind CAPRIN1 and APP and enhance the protein-protein interaction.
- Treatment of the degrader compounds induces CAPRIN1-mediated APP degradation through the endosomal-lysosomal pathway in AD iPSC neurons and organoids.
- The APP degraders provide new therapeutics through targeted protein degradation of APP and thereby disruption of the amyloid cascade in AD brain.

RESEARCH IN CONTEXT

1. **Systematic review:** Current literature indicates that targeted protein degradation is a rising strategy in drug discovery of small-molecule degraders that recruit disease-causing proteins to the proteasomal and lysosomal pathway for destruction. We have reported CAPRIN1-targeted small-molecule degraders and established CAPRIN1-targeted molecules library.

2. **Interpretation:** In screening of the library, we identified hit compound 0043 that degrades APP and reduces Aβ42 production in AD iPSC neurons. The structure-activity relationship (SAR) studies of 0043 analogs identified the more potent and drug-like lead compound 0152. The compounds act as molecular glues that bind CAPRIN1 and APP and enhance the protein -protein interaction. Tracking CAPRIN1 and APP through cellular organelles unveiled the mechanism of action of the degraders that induce CAPRIN1-mediated APP degradation through the endosomal-lysosomal pathway and thereby reduce Aβ peptide production and extracellular deposition in AD derived neurons and organoids.

3. **Future direction:** This study provides a proof-of-principle that small-molecule glues degrade APP and reduce Aβ using AD iPSC neuronal and organoid models. Further structure-activity relationship studies through chemical modifications of the compounds are necessary to identify more potent and blood brain barrier (BBB) permeable compounds for AD animal model studies and thereby preclinical development as the first-in-class drugs for treatment of AD patients.

1 Background

Alzheimer's disease (AD) is the most common cause of dementia [1]. The pathological hallmarks of AD include the accumulations of amyloid β (Aβ) peptides in extracellular plaques and the aggregations of hyperphosphorylated tau in neurofibrillary tangles in cerebral cortex and hippocampus [2]. The amyloid cascade hypothesis proposes that increased production and deposition of Aβ are the key central event that drives tau and other pathologies in AD [3, 4]. Aβ peptides are produced through sequential cleavage of amyloid-β protein precursor (APP) by β-secretase 1 (BACE1) and γ-secretase in neurons to release Aβ peptides extracellularly. The majority of Aβ has a length of 40 residues (Aβ40) but a small fraction of the longer Aβ42 is highly hydrophobic and prone to the accumulation and formation of extracellular plaques [5]. The increase in Aβ production is implicated in the pathogenesis of late-onset sporadic AD (sAD) and early-onset familiar AD (fAD) in which the mutations of *APP*, *presenilin 1* (*PSEN1*) and *PSEN2* lead to more Aβ42 production as well as the *APOE4* allele that results in less clearing of Aβ42 [6, 7]. Disease-modifying therapies have been developed to disrupt the amyloid cascade through inhibition of BACE1 and γ-secretase using enzymes inhibitors and clearance of Aβ amyloids from AD brain by Aβ-targeted monoclonal antibodies [3, 8]. Here, we provide a new disease-modifying therapeutic approach through targeted protein degradation of APP to reduce neuronal production and extracellular accumulation of Aβ42.

Targeted protein degradation is a rapidly rising strategy in drug discovery of degraders that recruit disease-causing proteins to the proteasomal and lysosomal pathway for destruction [9, 10]. Most well-known degraders are large multivalent compounds such as bifunctional proteolysis-targeting chimeras [11, 12]; but monovalent molecular glues are increasingly recognized as a distinctive set of small-molecule degraders that bind at the interface of two proteins and enhance

the protein-protein interaction and targeted protein degradation [13, 14]. Molecular glue degraders act on two proteins that already have a considerable affinity in proximity [15] and chemical modifications of the compounds enable derivatives to shift the substrate specificity and degrade a distinct set of substrate proteins, i.e. degrome [16]. Recently, we have reported small-molecule degraders of small ubiquitin-related modifier 1 (SUMO1), an undruggable oncoprotein [17]. SUMO1 degraders bind cytoplasmic activation/proliferation-associate protein 1 (CAPRIN1) and F-box protein 42 (FBXO42) to induce the recruitment of SUMO1, a substrate of FBXO42, to the cullin 1 (CUL1)-FBXO42 E3 ligase for SUMO1 ubiquitination and proteasomal degradation in cancers [18]. Noticing the proteomic finding of the affinity of CAPRIN1 and Aβ42 [19]. we screened our CAPRIN1-targeted molecules library [18] and identified the hit compounds 0043 and 0152 that were inactive on SUMO1 degradation but degrade APP and reduce Aβ production.

Human induced pluripotent stem cells (iPSCs) have accelerated biomedical research and drug discovery of human diseases by providing disease-specific models [20]. The development of AD patient iPSC-derived neurons (iPSC-Ns) and organoids has provided neuronal cell and brain tissue culture models of this complex disease [21, 22]. Using sAD and fAD iPSC-Ns and iPSC-derived organoids, we found that CAPRIN1 is dominantly expressed and interacts with APP in human neurons; and the compounds 0043 and 0152 bind CAPRIN1 and APP and enhance their interaction and CAPRIN1-mediated degradation of APP through the endosomal-lysosomal pathway. Through induction of APP degradation, these small-molecule glue degraders reduce the neuronal production and extracellular deposition of Aβ42 and thus provide new targeted protein degradation therapeutics for AD.

2 Methods

2.1 Cell lines and human iPSCs

HEK293 cells were purchased from the American Type Culture Collection (ATCC). The human iPSC SAD2.3 (UCSD234i-SAD2-3) were purchased from Wicell, UKBi011A from European Bank for induced pluripotent stem cells, Sigma, AG25367, AG25370, AG27606, AG27608, AG27609, and AG27602 from Coriell.

2.2 iPSC-Ns differentiation

The human iPSC SAD2.3 (UCSD234i-SAD2-3; Wicell), UKBi011A, AG25367, AG25370, AG27606, AG27608, AG27609, and AG27602 were maintained and expanded on Matrigel (Growth factor reduced Matrigel matrix, Corning) in mTeSR1 complete medium (mTeSR1 medium + 5X supplement, Stem Cell Technologies). For iPSC-Ns transgene delivery, each iPSC lines was transduced with lentiviral particles for pLVX-UbC-rtTA-Ngn2:2A:Ascl1 (Addgene #127289) or pLVX-UbC-rtTA-Ngn2:2A: EGFP (Addgene #84777) [23, 24], followed by selection in the presence of puromycin (0.5 mg/ml, Gibco). To initiate conversion, the transgene delivered iPSCs were dissociated with StemPro™ Accutase™ (Gibco) and reseeded in Neuro culture media (Neurobasal media (Gibco), 2% B27 supplement (Gibco), 1X Glutamax (Gibco)) with doxycycline (2 µg/ml, Sigma-Aldrich) for 5 days and without doxycycline for 3 days [25].

2.3 Brain 3D organoid formation

For generating brain 3D organoids, the Lancaster's protocol [26] and Paşca's protocol [27] were used with minor modifications. In brief, 9,000 cells/ 100 µL of each well were seeded in Ultra-low attachment 96 well U-bottom plates (Sbio) supplemented with 10 µM of ROCK inhibitor. Next day, 100 µl of mTeSR1 was added and the cells were cultured as embryonic bodies (EB) for

5 days at 37°C in 5% CO_2 incubator. When the size of EB reached 400-600 µm, EBs were transferred into ultra-low binding 24 well (Corning) with 200 µl of neural differentiation medium (Neurobasal medium (Gibco), 2% B27, 1X Glutamax) with 2 µg/ml of Doxycycline and incubated for 5 days at 37°C in 5% CO_2 incubator until the size of EB was 700-800 µm. During this step, each EB was in its own well and culture medium was changed every day with fresh neural differentiation medium with Doxycycline. At day 10, the EB was embedded into 15 µl of 100% Matrigel (Corning) and the embedded EBs were cultured in neural differentiation medium without Doxycycline in 6 well ultra-low binding plates (Corning). In this step, each well of 6 well plates had 16 EBs and plates were incubated in stationary methods for 5 days at 37°C in 5% CO_2 incubator to expand neuroepithelial buds, followed by placing the plates on the orbital shaker (Benchmark Scientific) at 75 rpm at 37°C in 5% CO_2 incubator. Fresh medium was changed every 3 days.

2.4 HEK-APP695^{WT} cell line construction

Lentiviral plasmids for APP695^{WT} HEK293 were generated in the 3rd generation plasmid system through Vectorbuilder Company (pLV-Hygro-CMV-hAPP). HEK293T cells were transfected with targeting plasmid and 3rd generation packing plasmid (pMD2.G, pMDLg/pRRE; Addgene #12251, and pRSV-Rev; Addgene #12253) together using Lipofectamine 2000. HEK293 cells were infected with virus particles and selected with hygromycin B (200 µg/ml, Invitrogen). For single clone selection, the cells were reseeded in 96-well plates as single cells. Once expanded, clones were analyzed by ELISA for amyloid beta 42 (Aβ42) and by western blot for APP expression. For sgCAPRIN1 HEK293 cell lines, the guide RNA sequences of CAPRIN1 were cloned into LentiCRISPRv2 plasmid (Addgene #52961) according to protocol [28]. The sequences

for CAPRIN1 CRISPR are available in Supplementary Table 1. HEK293 cells were infected, selected with puromycin (1 µg/ml) for 2 days, single cell selection, and followed by western blot for CAPRIN1 knock-out verification.

2.5 Generation of *APP*^{Swe}-iPSC

CRISPR Cas9 mediated knock-in cell Clones of APP-Swedish mutation in AG27606 iPSCs were generated by Synthego Corporation (Redwood City, CA, USA). Briefly, Ribonucleoproteins containing the Cas9 protein and synthetic chemically modified sgRNA were electroporated into the cells along with a single-stranded oligodeoxynucleotide donor using Synthego's optimized protocol. Editing efficiency was assessed upon recovery using Sanger sequencing, 48 hours post electroporation. The resulting chromatograms were processed using Synthego Inference of CRISPR edits software (ice.synthego.com). Edited cell pools were seeded at 1 cell/well using a single-cell printer into 96 or 384 well plates to create monoclonal cell populations. All wells were imaged every 3 days to ensure expansion from a single-cell clone. Clonal populations were screened and identified using the PCR-Sanger-ICE genotyping strategy.

2.6 Cellular Thermal Shift Assay (CETSA)

For CETSA, as described previously [29], iPSC-Ns or APP695^{WT}-HEK were treated in the presence or absence of 0043 (100 µM) for 1 hour, trypsinized, washed and resuspended in 100 µl of PBS with protease inhibitors (600,000 cells/tube). Cells were incubated at their designated temperatures for 3 minutes, followed by 25°C for 3 minutes. Then, 1% NP40 was added to lyse the cells, followed by immediate snap freezing with liquid nitrogen and thawing using thermal

cycler at 25°C. This freezing and thawing cycle was repeated twice. The lysates were spun at 13,500 rpm for 20 minutes at 4°C and supernatant was harvested, for western blotting analysis.

2.7 Thermofluor Assay

For the Thermofluor assay, Huynh's protocol [30] was used with minor modifications. In brief, all proteins were used at a final concentration of 5 μM for this assay and GloMelt™ Thermal Shift Protein Stability Kit (Biotium) was used at final concentration of 0.5X. All experiments were carried out with QuantStudio 6 Flex (Applied Biosystems). SYBR was used as a reporter and ROX was used as a passive reference according to the manufacturer's directions. Melting curve data was exported, followed by analysis with Boltzmann's sigmoidal curve in Prism 9.

2.8 Cytotoxicity and cell viability assay

Cytotoxicity test was conducted using Neutral Red Uptake assay [31]. In brief, iPSC-Ns seeded in 96 well plates (1×10^5 cells/well) were treated dose-dependently for 5 days. Cells were washed with PBS containing $CaCl_2$ and $MgCl_2$ followed by the addition of Neutral red solution (40 ug/ml in PBS, Sigma-Aldrich) and incubation at 37°C for 3 hours. Cells were then washed with PBS containing $CaCl_2$ and $MgCl_2$ two times and de-stained using with Neutral red de-staining solution on plate shaker for 30 minutes, followed by reading at 540 nm with Microplate reader. Cell viability was determined using the CellTiter-Glo® Luminescent Cell Viability Assay (Promega) in accordance with manufacturer instructions. In brief, HEK cells were plated at 5×10^4 cells/well, iPSC-Ns at 1×10^5 cells/well in 96 well plates and treated with drugs at 10 μM for 48 hours.

2.9 Antibodies

The following antibodies were used for western blot: anti-beta-Amyloid, 1-16 (6E10, BioLegend, 803001), anti-beta-Amyloid, 1-42 (12F4, BioLegend, 805501), β-Amyloid (Cell Signaling Technology, 8243), TUBB3 (Proteintech, 66375-1-Ig), Biotin-anti-beta-Amyloid, 17-24 (4G8, BioLegend, 800704), Anti-Amyloid Precursor Protein, C-Terminal (Sigma-Aldrich, A8717), Anti-Human sAPPbeta (Tecan (IBL), JP18957), Presenilin 1 (Cell Signaling Technology, 5643), Presenilin 2 (Cell Signaling Technology, 9979), BACE1 (Abcam, ab2077), ADAM10 (Cell Signaling Technology, 14194), Nicastrin (Cell Signaling Technology, 5665), GGA1 (Proteintech, 25674-1-AP), SORLA (Proteintech, 22592-1-AP), CD10/Neprilysin (Cell Signaling Technology, 65534), CD107a (LAMP-1) (BioLegend, 328601; Fisher Scientific, PA1-654A), SOX2 (Proteintech, 11064-1-AP), His•Tag® (Millipore, 70796-3), anti-APP C-Terminal Fragment (BioLegend, 802803).

2.l0 Western blot analysis and immunoprecipitation

Cells were lysed in 1% triton X-100 buffer (50mM Tris (pH 7.4), 150mM NaCl, 10% glycerol, 1% Triton x100, 1 mM EDTA) or RIPA buffer (50 mM Tris (pH7.5) 150 mM NaCl, 0.5% NP40, 0.5% deoxycholate, 0.1% SDS) supplemented with 1 mM PMSF, protease and phosphatase inhibitors. For immunoprecipitation, cell lysates were incubated with the primary antibodies (1-2 µg) overnight at 4°C and mixed with protein G beads for 4 hours. The immunoprecipitants were washed with 1% triton X-100 buffer 3 times and eluted with 2X Laemmli buffer, followed by western blot.

2.11 Real time PCR

Total RNA was isolated using the RNeasy kit (Qiagen), followed by synthesis for cDNA with a reverse transcription reaction (Quantitect® Reverse Transcription kit). The sequences for APP and GAPDH are in Table S1. Quantitative PCR was performed on QuantStudio 6 Flex (Applied Biosystems). The expression levels of APP were normalized to the GAPDH mRNA levels and represented relative to the expression in control cells. The results were analyzed with the delta-delta-Ct methods.

2.12 Enzyme-linked immunosorbent assay (ELISA)

For 2D culture, iPSC-Ns or HEK-APP695^{WT} were treated with drugs. Secreted Aβ42 peptides were quantified using the Human Amyloid β1-42 human ELISA kit (Thermo Fisher) according to the manufacturer's protocol. For 3D organoids ELISA, tissue processing was performed as described [32] with minor modifications. In brief, organoids were lysed with RIPA buffer supplemented with Protease and Phosphatase inhibitors (Sigma-Aldrich). Then, samples were sonicated and incubated on ice for 30 minutes, followed by centrifugation at 13,000 rpm for 30 minutes at 4°C. The supernatants (soluble fractions) were collected, and the pellets (insoluble fractions) were lysed with UREA buffer (8M Urea, 50 mM Tris (pH7.5), 100 mM NaCl, supplemented with protease and phosphatase inhibitors). Total protein in the soluble fraction was determined using BCA assay (Thermo Scientific). The Aβ42 in both RIPA and UREA fractions were measured using the Human Amyloid β1-42 human ELISA kit. The results were standardized with the amounts of proteins by BCA assay results.

2.13 Immunofluorescence staining

Cells were grown on glass cover slips coated with 1% Matrigel and treated with drugs. Cells were washed, fixed, permeabilized, and blocked and incubated in primary antibodies diluted in blocking solution (1% v/v BSA solution/5% Goat serum in PBS containing 0.1% Triton-X 100) overnight at 4°C. The primary antibodies used in the study included: polyclonal Rabbit anti-CAPRIN1 (15112-1-AP, Proteintech), monoclonal mouse anti-APP (22C11, MAB348, Millipore sigma), monoclonal mouse anti-MAP2 (AP18, MA5-12826, Thermo Fisher Scientific), polyclonal rabbit anti-NANOG (PA1-097); polyclonal rabbit anti-Calnexin (10427-2-AP, Proteintech), polyclonal rabbit anti-ERGIC-53 (13364-1-AP, Proteintech), polyclonal rabbit anti-SEC31A (17913-1-AP, Proteintech), polyclonal rabbit anti-TMED9 (21620-1-AP, Proteintech), monoclonal rabbit anti-GM130 (D6B1, 12480S, Cell Signaling Technology), polyclonal rabbit anti-TGN46 (13573-1-AP, Proteintech), monoclonal rabbit anti-EEA1 (C45B10, 3288S, Cell Signaling Technology), monoclonal rabbit anti-Rab7 (D95F2, 9367S, Cell Signaling Technology); monoclonal rabbit anti-LAMP1 (D2D11, 9091S, Cell Signaling Technology). The cells were washed three times with PBS and incubated in secondary antibodies in blocking solution for 1 hour at room temperature (Alexa Fluor 488® Goat anti-Mouse IgG; Alexa Fluor 488® Goat anti-Rabbit IgG; Alexa Fluor 555® Goat anti-Mouse IgG; Alexa Fluor 555® Goat anti-Rabbit IgG), then washed with PBS, followed by HOECHST staining (Invitrogen) for 5 minutes and washed with PBS. The glass coverslips were put on a slide in mounting medium (VECTASHIELD) and the edges were sealed with coverslip sealant (BIOTIUM). Image data was captured and processed with a confocal microscope system (Olympus Fluoview FV1000) and ImageJ program.

For 3D organoids staining, organoids were fixed in 10% formalin overnight at room

temperature followed by incubation in 30% sucrose solution overnight at room temperature, embedded in optimal cutting temperature compound (OCT, FisherScientific) and kept at -80°C overnight. Frozen samples were sectioned at 10 µm using a cryostat (Leica) and mounted on microscope slides (Fisherbrand™ superfrost plus, FisherScientific). Prior to immunolabeling, sections were rinsed in PBS for 5 minutes, permeabilized for 30 minutes in PBS containing 0.3% Triton-X 100, blocked for 1 hour in PBS containing 5% BSA and 0.1% Triton-X 100, and incubated with primary antibodies diluted in the same blocking solution. Then, secondary staining, mounting, and imaging were followed.

2.14 Immunohistochemistry of 3D organoids and human AD patient brain samples

Immunohistochemistry was performed in the Department of Pathology and Laboratory Medicine. Autopsy samples of brain tissues of Alzheimer's disease patients were provided by Indiana Pathology Institute (Indianapolis, Indiana, USA) in accordance with protocols approved by the institute. Paraffin-embedded 3D organoids and human AD patient brain samples subjected to Hematoxylin and Eosin (H&E), synapses, GFAP, CAPRIN1 (polyclonal Rabbit anti-CAPRIN1, 15112-1-AP, Proteintech), APP (monoclonal mouse anti-APP/Aβ (6E10), 803001, Biolegend; MAB348, Millipore sigma) in a Dako automated instrument using the Dako Flex detection system. The primary antibodies and secondary antibodies were used in colocalization experiments with human AD brain biopsy samples, then imaged using a confocal microscope system.

2.15 Imaging Analysis

ImageJ (Fiji) program (NIH, Bethesda, MD, USA) was used to analyze images [33]. Pearson's

correlation coefficients were calculated with JACop plugin from two channels. For trafficking analysis with organelles in iPSC-Ns, APP or CAPRIN1 or organelles signals were segmented using trainable weka segmentation plugin in Fiji. Colocalized area were calculated in image calculator tool ('Or' function) to get an overlayed area for the segmented signals, followed by using analyze particle tool in Fiji to determine by >1 pixel overlapping of segmented signal [34]. For colocalization analysis, APP, CAPRIN1, or LAMP1 were segmented by using trainable weka segmentation plugin for iPSC-Ns, HEK293 cells, and 3D organoids. To determine the fluorescence intensity, the corrected total cell fluorescence (CTCF) was used using the formula: CTCF = Integrated Density – (Area of selected cell x Mean fluorescence of background readings).

2.16 Recombinant proteins purification from E. coli

For full length CAPRIN1 purification, pET-6HIS-TEV-hCAPRIN1 (Vectorbuilder) were transformed into E. coli BL21 (DE3) followed by culturing in Luria broth (LB) with 100 µg/mL of Ampicillin overnight at 37°C. 10 ml of primary culture was inoculated into fresh LB medium with Ampicillin, cultured until OD600 reached 0.8, expression of CAPRIN1 was induced with 0.5 mM isopropyl-β-D-thiogalactoside at 37°C for 4 hours. After centrifugation at 3,000 rpm for 20 minutes at 4°C, pellets were dissolved with prechilled lysis buffer (50 mM Na_2HPO_4, 300 mM NaCl, 10% Glycerol, 0.1% Triton X-100, 10 mM Imidazole at pH 8.0), followed by sonication for 16 minutes (10 seconds on and 30 seconds off for 24 cycles) on ice and centrifuged for 40 minutes (40,000 rpm at 4°C). The supernatant was mixed with Ni-NTA agarose beads (Qiagen) overnight at 4°C, then loaded on a PD-10 column (GE healthcare). The columns were washed with buffer (50 mM Na_2HPO_4, 300 mM NaCl, 10% Glycerol, 10 mM Imidazole at pH 8.0) and eluted with elution buffer (50 mM Na_2HPO_4, 300 mM NaCl, 10% Glycerol, 250 mM Imidazole at pH 8.0),

followed by dialysis (50 mM Na_2HPO_4, 250 mM NaCl, 10% Glycerol at pH 8.0) for 2 hours at 4°C. The samples were concentrated using Millipore Amicon filters (Millipore) and dialyzed with storing buffer (50 mM Na_2HPO_4, 200 mM NaCl, 50% Glycerol at pH 8.0) for storing at -80°C.

For ^{15}N-CAPRIN1 samples for NMR, pCold-II-Halo-His8-HRV3C-CAPRIN1$^{112-260}$ plasmid were gifted from Du [35]. Plasmid transformed into E. coli BL21(DE3) cells and cultured overnight at 37°C. A single colony was selected and inoculated into 100 ml LB with 100 µg/mL Ampicillin overnight at 37°C for primary culture. The primary culture was then added to 1 L LB medium with Ampicillin (final OD600: 0.1) and was incubated at 37°C until OD600 0.8 at 37°C. Cells were then harvested and resuspended with 1 L ^{15}N-M9 minimal media (7.52 g of Na_2HPO_4-$2H_20$, 3 g of KH_2PO_4, 0.5 g of NaCl, 0.5 g of NH_4Cl, 50 mg of EDTA, 8.3 mg of $FeCl_3$-$6H_20$, 0.84 mg of $ZnCl_2$, 0.13 mg of $CuCl_2$-$2H_20$, 0.1 mg of $CoCl_2$-$2H_20$, 0.1 mg of H_3BO_3, 0.016 mg of $MnCl_2$-$4H_20$, 1g of $^{15}NH_4Cl$, 1 mM $MgSO_4$, 1 mM $CaCl_2$, 1 mg of Thiamine-HCl, 1 mg of Biotin, and 100 µg/ml Ampicillin), followed by shaking incubation overnight at 10°C. Cells were harvested at 3,500 rpm for 20 min at 4°C and resuspended with lysis buffer (50 mM Tris, 500 mM NaCl, 20 mM Imidazole, and 2 mM β-mercaptoethanol at pH 8.0), sonicated for 20 minutes (5 s on and off cycles) on ice, and centrifuged at 40,000 rpm for 40 minutes at 4°C. Then, Ni-NTA beads were added into supernatant and rotated overnight at 4°C, loaded on a PD-10 column. Beads were washed with lysis buffer and eluted with elution buffer (50 mM Tris, 500 mM NaCl, 300 mM Imidazole, and 2 mM β-mercaptoethanol at pH 8.0), followed by dialysis with buffer (50 mM Tris, 100 mM NaCl, and 0.5 mM β-mercaptoethanol at pH 8.0). Then, HRV3C protease (TAKARA) was added overnight at 4°C and Ni-NTA was added to eliminate the cleaved portion overnight at 4°C. The flow-through was harvested and fractionated by NGC Chromatography Systems (Bio-Rad) with buffer (50 mM Tris, 50 mM NaCl, and 0.5 mM β-mercaptoethanol at pH 8.0), followed

by concentration and cutoff using Millipore Amicon filters.

2.17 *In vitro* binding assay

When CAPRIN1 was used as a bait, recombinant CAPRIN1 (200 ng) was mixed with anti-CAPRIN1 antibodies (1µg) in IP buffer (25 mM Tris, 150 mM NaCl, 5% Glycerol, and 1% Triton X-100 at pH 7.4) overnight at 4°C, followed by the addition of Protein-G agarose beads for 4 hours at 4°C. CAPRIN1 conjugated beads were then washed with binding buffer (20 mM HEPES, 100 mM NaCl, 0.01% Triron X-100, and 5% Glycerol at pH 7.25) before the addition of recombinant human APP (prey) for 1 hour at 4°C. Beads were washed and eluted with 2X Laemmli buffer with boiling. When APP was used as a bait, biotin conjugated APP antibody (1 µg; 4G8, Biolegend) was pre-mixed with recombinant APP (100 ng, Biolegend) in pulldown buffer (0.1% NP-40, 50 mM Tris, 150 mM NaCl, 0.2 mM EDTA, 100 mM KCl, 1 mM $MgCl_2$, 0.2 mM $CaCl_2$, and 10% glycerol) overnight at 4°C, followed by addition of 0.5 mg of Streptavidin magnetic beads (Pierce) for 1 hour at 4°C. After washing the beads, recombinant human CAPRIN1 (full length, 100 ng) was added together with dose dependent 0043 in the binding buffer for 1 hour at 4°C. Beads were washed and eluted with 2X Laemmli buffer with boiling.

2.18 Nuclear magnetic resonance (NMR) spectroscopy

All NMR spectroscopy was performed at the Indiana University at Indianapolis on a Bruker Avance-III-600 NMR spectrometer operating at 600.2 MHz (1H), 61.081MHz (15N), and 150.9MHz (13C) and equipped with a TCI cryoprobe. All experiments were conducted at 298K in 5mm diameter NMR tubes with a sample volume of 500 µL. Solutions were buffered using

150 mM Potassium phosphate (pH 7.5) and 100 mM KCl dissolved in 90% H_2O and 10% D_2O. For WaterLOGSY, 20 µM of unlabeled CAPRIN1$^{112-260}$ protein and 200 µM of compound were used, and the mixing time was set to 1.5 s. The data was collected with 256 scans, a sweep width of 10ppm, an acquisition time of 1.58 s, and a relaxation delay 5 seconds. Prior to Fourier transformation the data were multiplied with an exponential function with a line broadening of 1 Hz. For ^{1}H-^{15}N HSQC experiments, 100 µM of ^{15}N-CAPRIN1$^{112-260}$ was used in free form as well in 0043 (200 µM) bound form. All spectra were processed using Bruker Topspin 4.1 software and analyzed using CARA (http://wiki.cara.nmr.ch/). The amide CSPs between free and bound states were calculated as CSP = $[(\delta Hfree - \delta Hbound)^2 + ((\delta Nfree - \delta Nbound)/5)^2]^{1/2}$, where δH and δN are the chemical shift of the backbone amide proton and nitrogen, respectively.

2.19 Recombinant CAPRIN1, APP695 and APP624 from insect cells

The DNA cassette (10xHis-3C site or 10xHis-MBP-3C site) was inserted immediately 5' of the *Bam*HI site in the pFastBac vector (Invitrogen, 10360014) using the SLIC method [36], yielding constructs termed pSEP0(10His-3C) (pYT1353), or pSEP8 (10His-MBP-3C) (pYT1566) vector respectively. The open reading frame (ORF) of human CAPRIN1 was codon-optimized, synthesized, and sub-cloned into the BamHI and HindIII site of a pSEP0 vector, yielding pSEP0-CAPRIN1 (10xHis-3C-CAPRIN1) (pYT1837) vector. The open reading frame (ORF) of a full-length human APP (APP695) was codon-optimized, synthesized, and sub-cloned into the BamHI and HindIII site of a pSEP8 vector, yielding pSEP8-APP695 (10xHis-MBP-3C-APP695) (pYT1842) vector. STOP codon was introduced into ORF of APP695 in pSEP8-APP695 construct, yielding pSEP8-APP624 vector (pYT1841) by which the C-terminal truncated mutant APP, APP624, was generated. Generation of baculovirus expressing 10xHis-CAPRIN1, 10xHis-MBP-

APP695, or 10xHis-MBP-APP624 using pSEP0-CAPRIN1, pSEP8-APP695, or pSEP8-APP624 vector in Sf9 cells (Expression Systems, Inc) was performed as described previously [37]. Expression of recombinant CAPRIN1, or APP695, or APP624 was optimized using the TEQC method [37] in which a 200 ml culture of Hi5 cells (Expression Systems, Inc, 94-002S) was infected at an estimated multiplicity of infection (eMOI) of 4. After a 96-hour incubation at 27°C, cells were harvested, frozen in liquid nitrogen and kept at -80°C until use.

For the purification of CAPRIN1, cell pellet was lysed in 50 mM Hepes-KOH pH 7.6, 400 mM potassium chloride (KCl, 10 % Glycerol, 5 mM β-mercaptoethanol, 10 mM Imidazole, and 0.5 ml of 100X protease cocktail (6 mM Leupeptin, 0.2 mM Pepstatin A, 20 mM Benzamidine, and 10 mM PMSF). Cell lysate was stirred for 30 min followed by centrifugation at 100,000 g for 45 min. The supernatant was loaded onto Ni-resin (HIS-Select, Sigma-Aldrich) and washed with buffer 1 (50 mM Hepes-KOH pH7.6, 1 M KCl, 5% Glycerol, 10 mM Imidazole, and 5 mM β-mercaptoethanol), and buffer 2 (50 mM Hepes-KOH pH7.6, 2 M KCl, 5% Glycerol, 10 mM Imidazole, and 5 mM β-mercaptoethanol) followed by lysis buffer and the low salt buffer (50 mM Hepes-KOH pH7.6, 200 mM KCl, 5% Glycerol, 10 mM Imidazole, and 5 mM β-mercaptoethanol). 10xHis-CAPRIN1 was eluted from Ni-resin with the elution buffer (50 mM Hepes-KOH pH7.6, 200 mM potassium acetate, 5% Glycerol, 300 mM Imidazole, and 5 mM β-mercaptoethanol). Elution fractions containing 10xHis-CAPRIN1 were pooled and dialyzed overnight against the low salt buffer. Dialysate was concentrated by spin column (Amicon 10k cut-off) to 4.0 mg/ml. Recombinant CAPRIN1 was further purified by 10–30% (v/v) glycerol gradient containing the buffer (50 mM Hepes-KOH pH7.6, 200 mM KCl, 5% glycerol and 5 mM β-mercaptoethanol). After centrifugation at 35,000 rpm in a Beckman SW Ti-40 rotor for 19 hours at 4°C, the gradient was fractionated using a PGF Piston Gradient Fractionator (BioComp Instruments). Fractions

containing 10xHis-CAPRIN1 were pooled and dialyzed overnight against the low salt buffer. Dialysate was concentrated by spin column (Amicon 10k cut-off) to 4 mg/ml. Concentration of purified protein was measured by Bradford method. When purifying APP695 and APP624, the same procedure as the CAPRIN1 purification was used. Buffer 1 (50 mM Hepes-KOH pH7.6, 1 M KCl, 5% Glycerol, 5 mM β-mercaptoethanol, and 0.1% DDM), wash buffer 2 (50 mM Hepes-KOH pH7.6, 2 M KCl, 5% Glycerol, 5 mM β-mercaptoethanol, and 0.1% DDM), low salt buffer with 0.1% DDM, elution buffer (50 mM Hepes-KOH pH7.6, 200 mM potassium acetate, 5% Glycerol, 50 mM Maltose, and 5 mM β-mercaptoethanol), and Amylose-resin were used.

2.20 CAPRIN1-APP interaction by glycerol gradient

~1 mg of 10xHis-MBP-APP695 or 10xHis-MBP-APP624, was mixed with ~1 mg of 10xHis-CAPRIN1 and loaded onto 10–30% (v/v) glycerol gradient containing the buffer (50 mM Hepes-KOH pH7.6, 200 mM KCl, 5 mM β-mercaptoethanol, and 0.1% DDM). For controls, ~1 mg of 10xHis-MBP-APP695 (full-length) or 10xHis-MBP-APP624, alone was loaded onto 10-30% (v/v) glycerol gradient as well. After centrifugation at 35,000 rpm in a Beckman SW Ti-40 rotor for 19 hours at 4°C, the gradient was fractionated as described above. For fractions containing 10xHis-CAPRIN1, a PGF Piston Gradient Fractionator was used. Fractions containing 10xHis-CAPRIN1, 10xHis-MBP-APP695 or 10xHis-MBP-APP624 alone or mixture were subjected to 4-12% NuPAGE (Invitrogen) and stained with Coomassie blue.

2.21 Statistics

Statistical analysis was performed with GraphPad Prism 9.0. The graphs originated from data were

presented as mean ± SD. A t-test, one-way analysis of variance (ANOVA) with Tukey's multiple comparisons test, and two-way ANOVA were used. Boltzmann's sigmoidal curve was used in CETSA graph. P values were reported as follows: *P < 0.05, **P < 0.01, ***P < 0.001, and ****P < 0.0001.

2.22 Synthesis of 0043 and 0152

Step 1 of 0043 synthesis. Methyl 2-amino-1,3-benzthiazole-6-carboxylate (2g, 9.6mmol) was suspended in THF (60mL) and reacted with 3-isocyanatobenzonitrile (1.65g, 11.5mmol) at 25°C for 16hr. TLC was run in 1:1 EtOAc/Hex to show completion. The reaction was concentrated then diluted with 40mL of EtOH. After heating the reaction mixture to 70°C, 40mL of CH_2Cl_2 was added and the reaction was stirred for 30mins. The solid was then cooled to 25°C, filtered and rinsed with EtOH to give 2.8g of methyl 2-[(3-cyanophenyl)carbamoylamino]-1,3-benzothiazole-6-carboxylate as a white solid (83%).

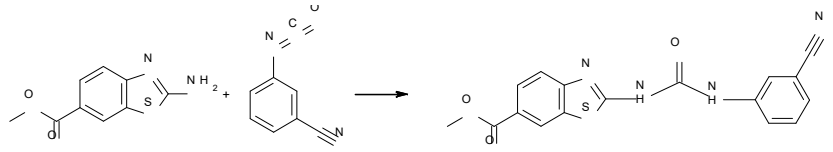

Step 2. Methyl 2-[(3-cyanophenyl)carbamoylamino]-1,3-benzothiazole-6-carboxylate (2.8g, 7.9 mmol) was suspended in a 2:1 solution of THF/EtOH (80mL). An aqueous 1N LiOH solution (58.1mmol) was added to the reaction and stirred at 25°C for 2 days. TLC in 1:1 EtOAc/Hex showed completion. The reaction was concentrated to remove the organic solvents and was diluted with 20mL of H_2O and 80mL of Isopropyl alcohol. The pH was adjusted to 5 using AcOH and after stirring for 1hr, the reaction was filtered and rinsed with Isopropyl alcohol

to obtain 2.3g (88%) of 2-[(3-cyanophenyl)carbamoylamino]-1,3-benzothiazole-6-carboxylic acid as a white solid.

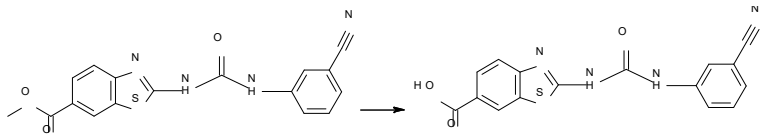

Step 3. 2-[(3-cyanophenyl)carbamoylamino]-1,3-benzothiazole-6-carboxylic acid (2.3g, 6.8 mmol) was suspended in DMF (90mL), then EDCI (2.1g, 13.6 mmol) and HOBT (1.1g, 8.16 mmol) were added to the reaction. After stirring at 25°C for 10mins, morpholine (2.9g, 34 mmol) and triethylamine (9.4 mL, 68 mmol) was added, then the reaction for stirred for 2 days at 25°C. TLC in 1:1 EtOAc/Hex showed completion, the reaction was poured into 200mL of H_2O and washed three times with 200mL of EtOAc. The organic washes were combined and concentrated to ~100mL and 100mL of H_2O was added. The organic and aqueous were left alone for 8hrs until white solid crashed out of solution. The solid was then filtered and rinsed with H_2O to give the title compound HB0043 (1.2 g, 43%) as a white solid.

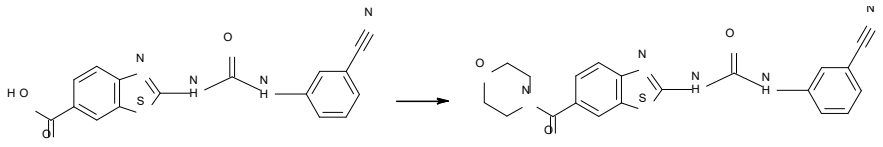

Step 1 of 0152 synthesis. Methyl 2-amino-1,3-benzthiazole-6-carboxylate (2g, 9.6mmol) was suspended in THF (60mL) and reacted with 1-methoxy-3-isocyanato-benzene (1.72g, 11.5mmol) at 25°C for 16hr. TLC was run in 1:1 EtOAc/Hex to show completion. The reaction was concentrated then diluted with 40mL of EtOH. After heating the reaction mixture to 70°C, 40mL of DCM was added and the reaction was stirred for 30mins. The solid was then cooled to 25°C, filtered and rinsed with EtOH to give 2.6g of Compound A as a white solid (76%).

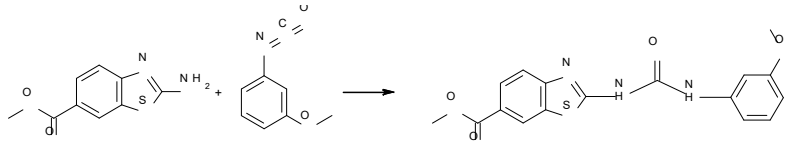

Step 2. Compound A (2.6g, 7.3mmol) was suspended in a 2:1 solution of THF/EtOH (80mL). An aqueous 1N LiOH solution (58.1mmol) was added to the reaction and stirred at 25°C for 2 days. TLC in 1:1 EtOAc/Hex showed completion. The reaction was concentrated to remove the organic solvents and was diluted with 20mL of H2O and 80mL of IPA. The pH was adjusted to 5 using AcOH and after stirring for 1hr, the reaction was filtered and rinsed with IPA to obtain 2.42g (97%) of compound B as a white solid.

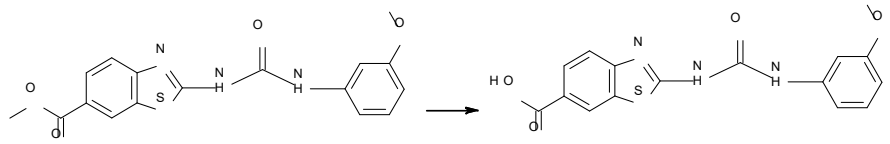

Step 3. Compound B (2.42g, 7.3mmol) was suspended in DMF (90mL), then EDC (2.8g, 14.6mmol) and HOBT (1.19g, 8.78mmol) was added to the reaction. After stirring at 25°C for 10mins, morpholine (2.55g, 29.3mmol) and triethylamine (8.21mL, 58.5mmol) was added, then the reaction for stirred for 2 days at 25°C. TLC in 1:1 EtOAc/Hex showed completion, the reaction was poured into 200mL of H2O and washed three times with 200mL of EtOAc. The organic washes were combined and concentrated to ~100mL and 100mL of H2O was added. The organic and aqueous were left alone for 8hrs until white solid crashed out of solution. The solid was then filtered and rinsed with H_2O to give 0152 (800mg, 27%) as a white solid of 0152.

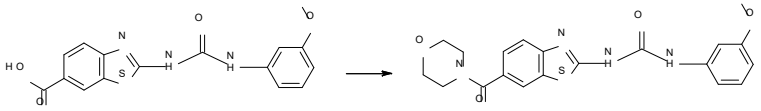

3 Results

3.1 Identification of CAPRIN1-targeted molecules that reduce Aβ42 and APP

To establish a cell model in screening of CAPRIN1-targeted molecules library, we expressed wild type APP695 ($APP695^{WT}$), a predominant form in human neurons [38] in human embryonic kidney 293T (HEK) cells [39]. APP is cleaved by BACE1 and γ-secretase to release Aβ42 extracellularly (Figure S1A) [40]; thus, ELISA was used to measure extracellular Aβ42 levels in culture medium [41]. In screening of our CAPRIN1-targeted molecules library [18], the stable HEK-$APP695^{WT}$ clone #2 was selected for the marked extracellular release of Aβ42 (Figure S1B). The clone was treated with each molecule; the culture medium was subsequently tested by ELISA for Aβ42. Cell viability was evaluated to eliminate compounds toxic to the cells (Figure S1C). The results identified seven active molecules that significantly reduced extracellular levels of Aβ42 (Figure 1A).

These seven active compounds identified share three pharmacophore motifs: a bicyclic ring, a urea core, and a phenyl ring (Figure 1B). The urea core was consistent in all the compounds. For the bicyclic ring, the 6-5 ring system was the most preferred for the activity with a benzothiazole ring such as 0043 being most active. Semi-saturated rings such as hexahydro-1,3-benzothiazole and hexahydrothiazolo [5,4-c]pyridine also preserve compound activity. For the phenyl ring moiety, carbonyl group in the meta-position of the ring improved the activity. Five out of seven active compounds contained a carbonyl moiety such as a tertiary amide or an ester on the phenyl ring. Of the seven active compounds, 0043 was more potent in a dose-dependent manner (Figure 1C) and its activity was not affected by fetal bovine serum (FBS) levels in medium (Figure S1D).

To evaluate the activity of the compounds on APP, western blots determined that 0043 treatment of HEK-$APP695^{WT}$ reduced APP but no BACE1, PSEN1, and presenilin enhancer 2

(PEN2) (Figure 1D). 0043 treatment reduced APP in dose-dependent manner (Figure 1E) but had no effects on the levels of CAPRIN1 and its binding partner Ras GTPase-activating protein-binding protein 1 (G3BP1) [42] (Figure 1F). The activity of 0043 on APP degradation was confirmed by western blots using the C-terminal antibody in HEK-APP695^{WT} cells (Figure 1G). In contrast, the mRNA levels of APP were not significantly changed by 0043 (Figure S1E). In contrast to the CAPRIN1-targeted SUMO1 degrader HB007 that inhibits cancer cell growth through degradation of SUMO1 [18], 0043 treatment had no effects on cancer cell growth and SUMO1 protein levels in cancer cells (Figure S1F-H). Moreover, 0043 treatment had no effects on APP levels in cancer cells in part due to the lack of APP expression in cancer cells as compared with AD iPSC-Ns (Figure 1H). Collectively, the results suggest that the hit compound 0043 reduces Aβ42 through induction of APP degradation in the cells.

3.2 The hit compound 0043 degrade APP and reduces Aβ42 production in AD-iPSC-Ns

To determine the activity of the compounds in AD, we differentiated human neurons from a panel of human iPSCs from sAD, fAD, and non-AD patients (Figure S2A), using the Ascl1/Mash1 [43] and Neurogenin 2 (Ngn2) protocol [44]. iPSCs were infected with Ngn2/Ascl1 and induced to differentiated neurons by doxycycline either in continuous or discontinuous treatment [25] (Figure S2B). ELISA detected higher Aβ42 levels in culture under discontinuous than continuous treatment (Figure 2A). All iPSCs were successfully differentiated to mutual iPSC-Ns, as determined by the stemness marker NANOG and the neuronal marker MAP2, respectively (Figure S2C, D).

The active compounds, as identified using HEK-APP695^{WT} cells, were tested first using sAD-iPSC SAD2.3-differentiated neurons (SAD2.3-Ns). ELISA confirmed the activity of 0043,

0047, 0048 and 0062 on reduction of extracellular Aβ42 (Figure 2B), but cell viability revealed the toxicity of 0062 to SAD2.3-Ns (Figure 2C). The compound 0043, 0047 and 0062 were further tested in all iPSC differentiated neurons (iPSC-Ns). The results showed that 0043 treatment reduced the extracellular Aβ42 in all iPSC-Ns, and to a greater extent in AD-iPSC-Ns compared to non-AD iPSC-Ns (Figure 2D). The data showed that fAD-iPSC-Ns with *PSEN1*, *PSEN2* mutation and *APOE4* allele were responsive to the compounds. To evaluate how APP mutant neurons responded, the wild type *APP* gene (APP^{WT}) in sAD-AG27606 iPSCs was edited by CRISPR-Cas9 to the Swedish APP mutant K595N/M596L [45]. The APP-Swedish mutation (APP^{SWE}) did not affect the neuronal differentiation of AG27606-iPSCs (Figure 2E), nor the mRNA expression of APP, nor the protein expression of APP, CAPRIN1 and BACE1 (Figure S2E, F). The APP^{SWE}, however, resulted in more than four times of extracellular release of Aβ42 (Figure 2F), consistent with the previous finding [46]. Treatment with 0043 significantly reduced extracellular release of Aβ42 from the APP^{SWE} neurons as compared with APP^{WT} AG27606-iPSCs (Figure 2G).

The activity of 0043 in Aβ42 reduction was dose and time-dependent with the IC_{50} values of the compound activity approximately at 1.8 μM and 2.1 μM, respectively, in the treatment of SAD2.3-Ns and AG27606-Ns (Figure 2H, I). Western blots showed that 0043 treatment of SAD2.3-Ns reduced intraneuronal APP, but not other AD related proteins such as BACE1, ADAM10 (constitutive α-secretase), PSEN1, nicastrin, ADP ribosylation factor-binding protein 1 (GGA1, BACE1 binding protein), Sorla (an intracellular sorting receptor to APP) and neprilysin in SAD2.3-iNs (Figure 2J). The activity of 0043 in APP reduction in SAD2.3-Ns and AG27606-Ns was dose-dependent (Figure 2K). In contrast, 0043 had no effects on the differentiation of SAD2.3 iPSCs in sAD2.3-iPSC-Ns or the mRNA transcriptional levels of *APP* gene in SAD2.3-

Ns and AG27600-Ns (Figure S2G, H). These studies have characterized the compound 0043 as an APP degrader that reduces extracellular Aβ42 in both sAD and fAD-iPSC-Ns.

3.3 The compound 0043 as a molecular glue directly binds CAPRIN1 and APP

To determine if the APP degrader 0043 binds CAPRIN1 like the SUMO1 degrader HB007 [18], we expressed and purified the recombinant human fragment of CAPRIN1 (rhCAPRIN1$^{112\text{-}260}$). The sensitive ligand-protein one-dimensional nuclear magnetic resonance (1D-NMR)-based water Ligand Observed via Gradient SpectroscopY (WaterLOGSY) [47] showed the difference in peak intensities due to different tumbling rates of the compound 0043 in presence or absence of rhCAPRIN1$^{112\text{-}260}$, indicating the binding of 0043 on rhCAPRIN1$^{112\text{-}260}$ (Figure 3A). To test the binding further, ^{1}H-^{15}N HSQC studies on isotopically ^{15}N-labelled rhCAPRIN1$^{112\text{-}260}$ were conducted based on the protocol reported [48], and the changes were monitored in presence of 0043; the results indicated significant chemical shift perturbations (CSPs) for some amide cross-peaks of CAPRIN1 in the presence of 0043, which confirmed the binding of 0043 on CAPRIN1 (Figure 3B and Figure S3A). Next, we conducted ThermoFluor assay and showed that the presence of 0043 stabilized CAPRIN1 upon binding and resulted in thermal shift (Figure 3C). To determine if 0043 also binds and stabilizes APP, we repeated ThermoFluor experiments with rhAPP^{695} and observed significant thermal shifts for rhAPP^{695} in the presence of 0043 (Figure 3D). The data indicate that 0043 directly binds CAPRIN1 and APP and thereby stabilize the proteins, which suggests that 0043 may act as a molecule glue between CAPRIN1 and APP.

To determine whether 0043 binds to cellular CAPRIN1 and APP, we conducted a cellular thermal shift assay (CETSA) [29, 49], in which CAPRIN1 and APP proteins, unlike PSEN1, showed a clear thermal stabilization with increase in temperature in the presence of 0043 in

AG27606-Ns (Figure 3E) and HEK-APP695^{WT} cells (Figure S3B). The presence of 0043 shifted the heat denaturation curve of CAPRIN1 and APP to higher temperatures, but not PSEN1 in AG27606-Ns (Figure 3F) or HEK-APP695^{WT} (Figure S3C). These results indicate that CAPRIN1 and APP are the binding partners of the compound 0043 in neurons. To confirm the role of CAPRIN1 in 0043-mediated degradation of APP, we generated *CAPRIN1* knockout (KO) clones from HEK-APP695^{WT} cells using a lentiCRISPRv2 system [28]. The sgCAPRIN1-KO HEK-APP695^{WT} clones were selected, as measured by western blots and immunofluorescence (Figure S3D, E). The clone was treated with 0043, western blots and ELISA showed that CAPRIN1 KO abolished the activity of 0043 on APP degradation in the cells and the extracellular release of Aβ42 (Figure 3G, H). These results indicate 0043 binds on CAPRIN1 and APP and induces CAPRIN1-mediated APP degradation in cells.

3.4 0043 binding of CAPRIN1 and APP enhances the protein-protein interaction

To investigate whether CAPRIN1 and APP interact with each other, we generated His-tagged rhCAPRIN1^{Full} (rhCAPRIN1) and His- and maltose-binding protein (MBP)-tagged rhAPP^{695}. The extracellular domain of APP was also generated without the transmembrane domain (rhAPP^{624}). To assess the stoichiometry of protein interaction, rhAPP^{624} or rhAPP^{695}, alone or mixed with rhCAPRIN1, were sedimented on glycerol gradient; and fractions of each sedimentation were analyzed by SDS-PAGE (Figure S4A, B). Mixing of rhCAPRIN1 and rhAPP resulted in the shift or spreading of the peak fractions of each protein towards higher molecular weights, suggesting one-to-one stoichiometric interaction of CAPRIN1 and APP (Figure 4A and Figure S4C). Immunoprecipitation of each fraction by anti-CAPRIN1 antibodies and western blots of immunoprecipitated fractions using an anti-MBP antibody confirmed the complex formation of

rhCAPRIN1 and rhAPP (Figure 4B and Figure S4D).

In evaluation of the role of 0043 on CAPRIN1 and APP interaction, biotinylated anti-APP antibody was used in pull down of HEK-APP695^{WT} cells and AG27606-Ns after treated with 0043. The results showed that 0043 treatment enhanced the interaction of CAPRIN1 and APP in HEK-APP695^{WT} and AG27606-Ns (Figure 4C, D). To test this at protein levels, we used biotinylated anti-APP antibody as a bait and rhCAPRIN1 or 0043 as a prey, western blot showed that 0043 increased biotinylated anti-APP antibody pull down of CAPRIN1 (Figure 4E). In a reverse, anti-CAPRIN1 antibody was used to pull down rhAPP^{695} and results showed that 0043 increased anti-CAPRIN1 antibody pull down of rhAPP (Figure 4F). Next, rhCAPRIN1 was coated on plates and incubated with rhAPP^{695} or rhAPP^{624} in the presence or absence of 0043. ELISA showed that 0043 increased the binding of both APP^{695} and APP^{624} to coated rhCAPRIN1 (Figure 4G). To determine the activity of 0043 in AD-iPSC-Ns, finally, AG27606-Ns were treated with 0043 and confocal fluorescent microscopy demonstrated that 0043 treatment increased the association of CAPRIN1 and APP in the neurons (Figure 4H, I). Collectively, these results indicate that 0043 acts as a molecular glue that enhances CAPRIN1 and APP interaction and CAPRIN1-mediated APP degradation in neurons.

3.5 Chemical modifications of 0043 identify the more potent and soluble lead compound 0152

To improve drug-like properties of 0043, we conducted structure-activity relationship (SAR) studies through chemical design, synthesis, and bioactivity analysis of 0043 derivatives. SAR results indicate that replacing the nitrile group with a methyl ether group significantly improved the drug-like properties of the derivative 0152 (Figure 5A). The mouse oral pharmacokinetics (PK) studies showed that the total drug exposure across time of the lead compound 0152, as determined

by the area under the curve (AUC), was 6 times higher than that of the hit compound 0043 and the oral bioavailability of 0152 was markedly improved up to 30% from 5% of 0043 (Figure 5B, C). To analyze the interaction of the lead compound 0152 and rhCAPRIN1, 1D NMR WaterLOGSY was recorded for the compound in the presence of rhCAPRIN1$^{112\text{-}126}$ and a change in peak intensities was observed, which confirmed the binding of 0152 on CAPRIN1 (Figure 5D). The compound 0152 was linked to biotin (0152-Biotin) and rhCAPRIN1 was incubated with 0152-Biotin; 0152-Biotin was subsequently pulled down by streptavidin-coated beads. Western blots of the pull-down confirmed the binding of rhCAPRIN1 to 0152-Biotin and the binding was inhibited competitively by free 0152 (Figure S5A). AG27606-Ns lysates were then included with 0152-Biotin and pull-down assay confirmed the binding of cellular CAPRIN1 and APP on 0152-Biotin while the binding was inhibited competitively by free 0152, but not free HB007 suggesting that 0152 and HB007 bind different sites of rhCAPRIN1 (Figure 5E).

To evaluate the activity of 0152 in AD iPSC-Ns, ELISA of Aβ42 in culture medium showed the improved potency of 0152 in reduction of extracellular Aβ42 release, as compared with the hit compound 0043 in sAD AG27606 and fAD UKBi011A iPSC-Ns (Figure 5F, G). AD-iPSC-Ns were then treated with a series of the dilutions of 0152; ELISA showed the improved IC50 values ranging from 0.8-0.9 μM of the lead 0152 as compared with the IC50 of the hit 0043 at 2 μM in Aβ42 reduction (Figure 5H, I). The potent activity of 0152 on reduction of extracellular Aβ42 levels was also confirmed using sAD2.3-Ns and APP^{SWE} mt AG27606-Ns (Figure S5B, C).

Western blots further confirmed that the treatment of 0152 markedly reduced APP levels in AG27606-Ns as compared with 0043 (Figure 5J). Confocal microscopy revealed that 0152 treatment increased CAPRIN1 and APP interaction in AG27606-Ns (Figure 5K) and sAD2.3-Ns (Figure S5D, E). Finally, CAPRIN1 KO sgCAPRIN1-HEK-APP695^{WT} clones were treated with

0043 and 0152; ELISA showed 0152 was more potent than 0043 in reduction of extracellular Aβ42; and western blots showed the significant reduction of APP levels (Figure S5F, G). In contrast, CAPRIN1 knockout drastically reduced the effects of 0043 and 0152 on both Aβ42 and APP reduction (Figure S5H). Collectively, these results establish 0152 as the lead compound of APP small-molecule degraders with improved drug-like properties and potent activity in induction of APP degradation and decrease of Aβ42 extracellular release.

3.6 APP degraders induce CAPRIN1-mediated APP lysosomal degradation in iPSC neurons

To reveal the mechanism of action, we determined whether the degraders induce APP degradation either through the proteasome or lysosome using the proteasome inhibitor MG132 and the lysosome inhibitor Bafilomycin A1 (Baf A1). The presence of MG132 had no effects on 0043-induced degradation of APP in AG27606-Ns (Figure 6A), sAD2.3-Ns and HEK-APP695^{WT} (Figure S6A, B). In contrast, Baf A1 pretreatment abolished the activity of 0043 in APP degradation in AG27606-Ns (Figure 6B), sAD2.3-Ns and HEK-APP695^{WT} (Figure 6C, D). The data suggest that the compound induces APP degradation through the lysosome. Next, we tracked APP through cellular organelles using confocal co-localization of APP and CAPRIN1 with organelle-specific markers (Figure S6E) [50, 51]. APP was colocalized with the earlier endosome antigen 1 (EEA1), the late endosome Rab7 and the lysosomal associate membrane protein 1 (LAMP1) in AG27606-Ns; while CAPRIN1 was co-localized with Rab7 and LAMP1, as well as SEC31A (Figure S6F, G), a subunit of the coat protein complex II (COPII) of the endoplasmic reticulum (ER) enriched with stress granules coated vesicle [52], consistent with previous reports [42]. The treatment of 0043 increased the co-localization of APP and CAPRIN1 with EEA1, Rad7 and LAMP1 (Figure 6C). The 0043-enhanced co-localization of LAMP1 was further confirmed in

a panel of AD-iPSC-Ns by confocal correlation coefficient analysis (Figure 6D, E and Figure S6H, I).

To further determine the role of CAPRIN1 on APP lysosomal degradation, we carried out immunoprecipitation of 0043-treated AG27606-Ns and UKBi011A-Ns by a CAPRIN1 antibody. Western blots of the immunoprecipitated showed that 0043 treatment increased CAPRIN1 pull-down of APP and LAMP1 in AD-iPSC-Ns (Figure 6F, G). AG27606-Ns were then treated with 0043 and 0152 and confocal microscopy showed the more potent activity of 0152 in enhancing of the colocalization of APP and LAMP1 in AD-iPSC-Ns (Figure 6H, I). CAPRIN1 knockout (KO) in sgCAPRIN1-HEK-APP695^{WT} drastically reduced the effects of 0043 and 0152 on the co-localization of APP and LAMP1 (Figure 6J and Figure S6J). Taken together, the results suggest that, through binding on CAPRIN1 and APP, the compounds 0043 and 0152 enhance CAPRIN1-mediated APP trafficking from the endosome to lysosome for APP degradation.

3.7 APP degraders reduce Aβ42 levels in AD iPSC-derived brain organoids

To define the role of CAPRIN1 in AD, we first examined CAPRIN1 expression and localization in AD brains. Immunohistochemistry (IHC) of paraffin embedded, and formalin fixed sections of autopsy brains demonstrated that CAPRIN1 and APP were predominantly expressed in neurons in AD and non-AD brains, whereas Aβ42 was extracellular in AD brains (Figure 7A, B). Confocal immunofluorescent stains of the section further showed the co-localization of CAPRIN1 and APP in neurons (Figure 7C). Next, we developed 3 dimensional (3D) organoids from AD iPSCs as AD brain tissue models (Figure S7A), based on the protocols [26, 27]. Hematoxylin and eosin (H&E) histochemistry and immunohistochemistry of paraffin embedded, and formalin fixed sections of

AG27606-3D organoids revealed the differentiation of neurons and astroglia as determined by neuronal synaptophysin and glial fibrillary acidic protein (GFAP) (Figure S7B). Confocal immunofluorescence stains of the sections of AG27606-3D organoids showed the expression of the neuronal marker MAP2 and TUJ1 and more accumulation of APP/Aβ in a long-term culture than shorter or healthy organoids (Figure S7C, D). Immunohistochemistry of AG27606-3D organoids demonstrated that CAPRIN1 and APP were dominantly expressed in organoids (Figure 7D), as shown in human AD brains. Immunofluorescent stains with confocal microscopy showed that the compound increased colocalization of APP and CAPRIN1 in the organoids after 1-month and 3-months treatments (Figure 7E, F); and the treatment of the compounds markedly reduced APP and Aβ in AD-3D-organoids as compared with the γ-secretase inhibitors (GSI, γ-Secretase Inhibitor XXI, Compound E) [53, 54] as control (Figure 7G, H and Figure S7E, F). The compounds decreased Aβ peptides was confirmed by the antibody that recognizes Aβ37-42 peptides in immunofluorescence microscopy and ELISA of Aβ42 (Figure S7G, H, I). These results indicated that compounds 0043 and 0152 induce APP and CAPRIN1 co-localization and APP degradation, thus resulting in Aβ reduction in AD iPSC derived organoids.

4 Discussion

In the past decades, anti-AD therapies have been focused on development of BACE1 and γ-secretase inhibitors in block of Aβ production, and Aβ-targeted monoclonal antibodies such as donanemab to clear amyloids [3, 8]. However, more than several hundreds of clinical trials of amyloid targeted therapeutics have been terminated because they are ineffective [55, 56]. Recently, clinical trials of new generation of Aβ-targeted monoclonal antibodies such as donanemab showed

that the antibodies reduces amyloid levels and slows cognitive decline in early symptomatic patients [57], a vindication for amyloid cascade as a therapeutic target in AD [58]. In this study, we discovered the first small-molecule degraders of APP and demonstrated that the APP degraders induce the production of Aβ peptides through induction of the lysosomal degradation of APP in AD iPSC derived neurons and brain organoids. By lowering the levels of APP and Aβ peptides in AD brain, APP degraders provide an alternative targeted protein degradation of APP for AD either as single agents or in combination of Aβ-targeted monoclonal antibodies that remove accumulated amyloids from AD brain.

The current concept in targeted protein degradation stipulate that molecule glue degraders act mostly on affinity proteins in proximity and compound modifications shift the affinity to other substrate proteins [15, 16]. The data presented here further suggest the novel concept that molecule glue degraders are selective in various types of cells, tissues, and diseases based on endogenous, cellular degradation pathways of targeted proteins. In cancer, for instance, CAPRIN1-targeted degraders of SUMO1 bind CAPRIN1 and FBXO42 and induces FBXO42 recruitment of SUMO1 to the FBXO42-CUL1 E3 ligase for SUMO1 degradation through the ubiquitin proteasome pathway [18]. On the other hand, however, CAPRIN1 interacts with APP in human neurons and CAPRIN1-targeted molecular glues that are inactive in SUMO1 degradation bind CAPRIN1 and APP and enhance the protein-protein interaction and promote CAPRIN1-mediated APP degradation through the endosomal-lysosomal pathway in AD neurons. The difference between the bioactivities of SUMO1 and APP molecular degraders is in part due to the expression of FBXO42-CUL1 E3 ligase and APP, respectively in cancer and neurons. The binding protein CAPRIN1, however, is highly expressed both in cancers [18] and neurons, as demonstrated here, and a systemic proteomic identified CUL1 and APP as the binding partners of CAPRIN1,

respectively in cancer and neurons [19, 59]. The competitive pull-down assays as presented here indicate that SUMO1 and APP molecule degraders bind at different sites on CAPRIN1. Structural studies of CAPRIN1-compound complexes will shed light on the mechanism of action of these two distinct molecular glue degraders.

The results presented here provide a previously unknown mechanism in which CAPRIN1-mediates APP lysosomal degradation in AD neurons and thereby identify CAPRIN1 and APP as molecule glue targets. CAPRIN1 has been reported in brain development and neurodegeneration [60]. CAPRIN1 and G3BP1 form a stable complex in stress granules responsible for neuronal synaptic formation [61] and *CAPRIN1* or *G3BP1* KO results in the death of newborn mice due to synaptic and respiratory failure [62, 63]. CAPRIN1 is involved in RNA metabolic response in stress granules in neurodegenerative diseases including AD [64]. Tracking CAPRIN1 through cellular organelles in AD iPSC neurons, we show that CAPRIN1 is localized in the stress granules and thus confirm its role in RNA metabolism in stress granules in developmental and neurodegenerative brains. Tracking CAPRIN and APP localizes both proteins in the endosomes and lysosomes. The endosomal-lysosomal pathway has been reported in APP processing and clearance and its dysfunction in APP degradation contributes to the pathogenesis of AD [65]. The data presented here indicate that CAPRIN1 interacts with APP and mediates APP degradation through the endosomal-lysosome pathway in AD neurons. By binding of CAPRIN1 and APP, the molecule glue degraders enhance CAPRIN1 and APP interaction and promote APP degradation through the endosomal-lysosomal pathway.

The current AD iPSC models of differentiated neurons and brain organoids [21, 22] have enabled us to prove the principle that molecule glues of CAPRIN1 and APP can reduce Aβ peptides through the targeted protein degradation of APP in neurons. However, the iPSC models have their

limitation, two being the lack in amyloid plaques and the absence of blood brain barrier (BBB). Numerous transgenic mouse models harboring fAD mutations have been established and exhibit the BBB and amyloid plaques of AD brain; however, the mechanism and response of drugs differ between mouse and human brains [66]. While molecular inhibitors target individual proteins, molecular glues bind two endogenous proteins in proximity [13, 14]. It is unclear whether CAPRIN1 interacts with APP and mediates APP lysosomal degradation in mice, as we demonstrate here in human neurons and brain organoids. It is necessary, therefore, to understand the mechanism of drug action in AD mouse models before the models can be used in evaluation of the therapeutic efficacy of the molecular glue compounds. In addition, our SAR studies of our molecular glue compounds are at the early hit to lead stage of drug discovery and development [67]. Further SAR studies through hit to lead optimization are necessary to identify more potent, drug-like and BBB permeable lead compounds for preclinical development as the first-in-class anti-aging drugs for clinical treatment of patients diagnosed with AD.

In conclusion, this study using AD iPSC neurons and organoids leads to the discovery of small-molecule glue degraders that bind CAPRIN1 and APP and reduce Aβ peptide production through CAPRIN1-mediated degradation of APP in the lysosome. The small-molecule glue degraders provide new therapeutics through targeted protein degradation of APP and disruption of the amyloid cascade in AD brain.

AUTHOR CONTRIBUTIONS

Anita C. Bellail and Chunhai Hao initiated the project, designed the experiments, and provided supervision. Sunghan Jung carried out all the drug screenings, molecular, biochemical and iPSC cellular experiments. Nancy Jaiswal and Ratan K. Rai performed NMR studies and data analysis.

Nancy Jaiswal, Yuichiro Takagi and Ryan K. Higgins expressed proteins. Ho-Yin Lo, Cen Gao, Lifan Zeng, Xu Wang designed, synthesized, purified, and analyzed compounds. Reagan K. Wohlford assisted the research. Sunghan Jung, Anita C. Bellail and Chunhai Hao analyzed and organized all the data and wrote the manuscript together. All authors helped editing the manuscript.

ACKNOWLEDGEMENTS

The authors acknowledge the assistance of the Chemical Genomics Core and the Indiana Center for Biological Microscopy of Indiana University School of Medicine. This work was supported in part by the Indiana University School of Medicine Physician Scientist Initiative funded by Lilly Endowment, Inc. (C.H.), and the research fund from the Department of Pathology & Laboratory Medicine of the Indiana University School of Medicine. C.H. has been supported in part by the endowment fund of the Bicentennial Chair of the Indiana University School of Medicine.

CONFLICT OF INTEREST STATEMENT

Anita C. Bellail and Chunhai Hao are the co-founders of HB Therapeutics, Inc. and Degrome Therapeutics, Inc. Ho-Yin Lo is the founder and an employee of Synovel Laboratory. The U.S. provisional patent application 63/611,294 entitled “Compounds and methods to treat Alzheimer’s disease” was filed by Indiana University. Other authors declare no conflict of interest.

REFERENCES

[1] Rajan KB, Weuve J, Barnes LL, McAninch EA, Wilson RS, Evans DA. Population estimate of people with clinical Alzheimer's disease and mild cognitive impairment in the United States (2020-2060). Alzheimers Dement. 2021;17:1966-75.

[2] Montine TJ, Phelps CH, Beach TG, Bigio EH, Cairns NJ, Dickson DW, et al. National Institute on Aging-Alzheimer's Association guidelines for the neuropathologic assessment of Alzheimer's disease: a practical approach. Acta Neuropathol. 2012;123:1-11.

[3] Karran E, De Strooper B. The amyloid hypothesis in Alzheimer disease: new insights from new therapeutics. Nat Rev Drug Discov. 2022;21:306-18.

[4] Rafii MS, Aisen PS. Detection and treatment of Alzheimer's disease in its preclinical stage. Nat Aging. 2023;3:520-31.

[5] Muller UC, Deller T, Korte M. Not just amyloid: physiological functions of the amyloid precursor protein family. Nat Rev Neurosci. 2017;18:281-98.

[6] Rosenberg RN, Lambracht-Washington D, Yu G, Xia W. Genomics of Alzheimer Disease: A Review. JAMA Neurol. 2016;73:867-74.

[7] Chavez-Gutierrez L, Bammens L, Benilova I, Vandersteen A, Benurwar M, Borgers M, et al. The mechanism of gamma-Secretase dysfunction in familial Alzheimer disease. EMBO J. 2012;31:2261-74.

[8] Oumata N, Lu K, Teng Y, Cave C, Peng Y, Galons H, et al. Molecular mechanisms in Alzheimer's disease and related potential treatments such as structural target convergence of antibodies and simple organic molecules. Eur J Med Chem. 2022;240:114578.

[9] Mullard A. Targeted protein degraders crowd into the clinic. Nat Rev Drug Discov. 2021;20:247-50.

[10] Paudel RR, Lu D, Roy Chowdhury S, Monroy EY, Wang J. Targeted Protein Degradation via Lysosomes. Biochemistry. 2023;62:564-79.

[11] O'Brien Laramy MN, Luthra S, Brown MF, Bartlett DW. Delivering on the promise of protein degraders. Nat Rev Drug Discov. 2023;22:410-27.

[12] Alabi SB, Crews CM. Major advances in targeted protein degradation: PROTACs, LYTACs, and MADTACs. J Biol Chem. 2021;296:100647.

[13] Schreiber SL. The Rise of Molecular Glues. Cell. 2021;184:3-9.

[14] Domostegui A, Nieto-Barrado L, Perez-Lopez C, Mayor-Ruiz C. Chasing molecular glue degraders: screening approaches. Chem Soc Rev. 2022;51:5498-517.

[15] Du X, Volkov OA, Czerwinski RM, Tan H, Huerta C, Morton ER, et al. Structural Basis and Kinetic Pathway of RBM39 Recruitment to DCAF15 by a Sulfonamide Molecular Glue E7820. Structure. 2019;27:1625-33 e3.

[16] Sievers QL, Petzold G, Bunker RD, Renneville A, Slabicki M, Liddicoat BJ, et al. Defining the human C2H2 zinc finger degrome targeted by thalidomide analogs through CRBN. Science. 2018;362.

[17] Bellail AC, Olson JJ, Hao C. SUMO1 modification stabilizes CDK6 protein and drives the cell cycle and glioblastoma progression. Nat Commun. 2014;5:4234.

[18] Bellail AC, Jin HR, Lo HY, Jung SH, Hamdouchi C, Kim D, et al. Ubiquitination and degradation of SUMO1 by small-molecule degraders extends survival of mice with patient-derived tumors. Sci Transl Med. 2021;13:eabh1486.

[19] Olah J, Vincze O, Virok D, Simon D, Bozso Z, Tokesi N, et al. Interactions of pathological hallmark proteins: tubulin polymerization promoting protein/p25, beta-amyloid, and alpha-synuclein. J Biol Chem. 2011;286:34088-100.

[20] Shi Y, Inoue H, Wu JC, Yamanaka S. Induced pluripotent stem cell technology: a decade of progress. Nat Rev Drug Discov. 2017;16:115-30.
[21] Blanchard JW, Victor MB, Tsai LH. Dissecting the complexities of Alzheimer disease with in vitro models of the human brain. Nat Rev Neurol. 2022;18:25-39.
[22] Bubnys A, Tsai LH. Harnessing cerebral organoids for Alzheimer's disease research. Curr Opin Neurobiol. 2022;72:120-30.
[23] Mertens J, Herdy JR, Traxler L, Schafer ST, Schlachetzki JCM, Böhnke L, et al. Age-dependent instability of mature neuronal fate in induced neurons from Alzheimer's patients. Cell Stem Cell. 2021;28:1533-48.e6.
[24] Herdy J, Schafer S, Kim Y, Ansari Z, Zangwill D, Ku M, et al. Chemical modulation of transcriptionally enriched signaling pathways to optimize the conversion of fibroblasts into neurons. eLife. 2019;8.
[25] Kondo T, Imamura K, Funayama M, Tsukita K, Miyake M, Ohta A, et al. iPSC-Based Compound Screening and In Vitro Trials Identify a Synergistic Anti-amyloid β Combination for Alzheimer's Disease. Cell reports. 2017;21:2304-12.
[26] Lancaster MA, Knoblich JA. Generation of cerebral organoids from human pluripotent stem cells. Nat Protoc. 2014;9:2329-40.
[27] Pasca AM, Sloan SA, Clarke LE, Tian Y, Makinson CD, Huber N, et al. Functional cortical neurons and astrocytes from human pluripotent stem cells in 3D culture. Nat Methods. 2015;12:671-8.
[28] Sanjana NE, Shalem O, Zhang F. Improved vectors and genome-wide libraries for CRISPR screening. Nat Methods. 2014;11:783-4.
[29] Jafari R, Almqvist H, Axelsson H, Ignatushchenko M, Lundback T, Nordlund P, et al. The cellular thermal shift assay for evaluating drug target interactions in cells. Nat Protoc. 2014;9:2100-22.
[30] Huynh K, Partch CL. Analysis of protein stability and ligand interactions by thermal shift assay. Curr Protoc Protein Sci. 2015;79:28 9 1- 9 14.
[31] Repetto G, del Peso A, Zurita JL. Neutral red uptake assay for the estimation of cell viability/cytotoxicity. Nature protocols. 2008;3:1125-31.
[32] Zhao J, Fu Y, Yamazaki Y, Ren Y, Davis MD, Liu CC, et al. APOE4 exacerbates synapse loss and neurodegeneration in Alzheimer's disease patient iPSC-derived cerebral organoids. Nat Commun. 2020;11:5540.
[33] Schindelin J, Arganda-Carreras I, Frise E, Kaynig V, Longair M, Pietzsch T, et al. Fiji: an open-source platform for biological-image analysis. Nature methods. 2012;9:676-82.
[34] Liao YC, Fernandopulle MS, Wang G, Choi H, Hao L, Drerup CM, et al. RNA Granules Hitchhike on Lysosomes for Long-Distance Transport, Using Annexin A11 as a Molecular Tether. Cell. 2019;179:147-64 e20.
[35] Wu Y, Zhu J, Huang X, Du Z. Bacterial expression and preliminary crystallographic studies of a 149-residue fragment of human Caprin-1. Acta crystallographica Section F, Structural biology communications. 2015;71:324-9.
[36] Li MZ, Elledge SJ. Harnessing homologous recombination in vitro to generate recombinant DNA via SLIC. Nature methods. 2007;4:251-6.
[37] Imasaki T, Wenzel S, Yamada K, Bryant ML, Takagi Y. Titer estimation for quality control (TEQC) method: A practical approach for optimal production of protein complexes using the baculovirus expression vector system. PLoS One. 2018;13:e0195356.

[38] Hick M, Herrmann U, Weyer SW, Mallm JP, Tschape JA, Borgers M, et al. Acute function of secreted amyloid precursor protein fragment APPsalpha in synaptic plasticity. Acta Neuropathol. 2015;129:21-37.
[39] Stachel SJ, Coburn CA, Steele TG, Jones KG, Loutzenhiser EF, Gregro AR, et al. Structure-based design of potent and selective cell-permeable inhibitors of human beta-secretase (BACE-1). J Med Chem. 2004;47:6447-50.
[40] Karran E, Mercken M, De Strooper B. The amyloid cascade hypothesis for Alzheimer's disease: an appraisal for the development of therapeutics. Nat Rev Drug Discov. 2011;10:698-712.
[41] Bell RD, Deane R, Chow N, Long X, Sagare A, Singh I, et al. SRF and myocardin regulate LRP-mediated amyloid-beta clearance in brain vascular cells. Nat Cell Biol. 2009;11:143-53.
[42] Wu Y, Zhu J, Huang X, Du Z. Crystal structure of a dimerization domain of human Caprin-1: insights into the assembly of an evolutionarily conserved ribonucleoprotein complex consisting of Caprin-1, FMRP and G3BP1. Acta Crystallogr D Struct Biol. 2016;72:718-27.
[43] Vierbuchen T, Ostermeier A, Pang ZP, Kokubu Y, Sudhof TC, Wernig M. Direct conversion of fibroblasts to functional neurons by defined factors. Nature. 2010;463:1035-41.
[44] Hulme AJ, Maksour S, Glover MSC, Miellet S, Dottori M. Making neurons, made easy: The use of Neurogenin-2 in neuronal differentiation. Stem Cell Rep. 2022;17:14-34.
[45] Haass C, Lemere CA, Capell A, Citron M, Seubert P, Schenk D, et al. The Swedish mutation causes early-onset Alzheimer's disease by beta-secretase cleavage within the secretory pathway. Nat Med. 1995;1:1291-6.
[46] Zhou B, Lu JG, Siddu A, Wernig M, Sudhof TC. Synaptogenic effect of APP-Swedish mutation in familial Alzheimer's disease. Sci Transl Med. 2022;14:eabn9380.
[47] Bataille CJR, Rabbitts TH, Claridge TDW. NMR waterLOGSY as An Assay in Drug Development Programmes for Detecting Protein-Ligand Interactions-NMR waterLOGSY. Bio Protoc. 2020;10:e3666.
[48] Barile E, Pellecchia M. NMR-based approaches for the identification and optimization of inhibitors of protein-protein interactions. Chem Rev. 2014;114:4749-63.
[49] Reinhard FB, Eberhard D, Werner T, Franken H, Childs D, Doce C, et al. Thermal proteome profiling monitors ligand interactions with cellular membrane proteins. Nat Methods. 2015;12:1129-31.
[50] Dvela-Levitt M, Kost-Alimova M, Emani M, Kohnert E, Thompson R, Sidhom EH, et al. Small Molecule Targets TMED9 and Promotes Lysosomal Degradation to Reverse Proteinopathy. Cell. 2019;178:521-35 e23.
[51] Gomez-Navarro N, Miller E. Protein sorting at the ER-Golgi interface. J Cell Biol. 2016;215:769-78.
[52] Zappa F, Wilson C, Di Tullio G, Santoro M, Pucci P, Monti M, et al. The TRAPP complex mediates secretion arrest induced by stress granule assembly. EMBO J. 2019;38:e101704.
[53] Wolfe MS. gamma-Secretase inhibitors and modulators for Alzheimer's disease. J Neurochem. 2012;120 Suppl 1:89-98.
[54] Shelton CC, Zhu L, Chau D, Yang L, Wang R, Djaballah H, et al. Modulation of gamma-secretase specificity using small molecule allosteric inhibitors. Proc Natl Acad Sci U S A. 2009;106:20228-33.
[55] Dolgin E. How to defeat dementia. Nature. 2016;539:156-8.

[56] Abbott A, Dolgin E. Failed Alzheimer's trial does not kill leading theory of disease. Nature. 2016;540:15-6.
[57] Sims JR, Zimmer JA, Evans CD, Lu M, Ardayfio P, Sparks J, et al. Donanemab in Early Symptomatic Alzheimer Disease: The TRAILBLAZER-ALZ 2 Randomized Clinical Trial. JAMA. 2023;330:512-27.
[58] Reardon S. Alzheimer's drug donanemab helps most when taken at earliest disease stage, study finds. Nature. 2023;619:682-3.
[59] Bennett EJ, Rush J, Gygi SP, Harper JW. Dynamics of cullin-RING ubiquitin ligase network revealed by systematic quantitative proteomics. Cell. 2010;143:951-65.
[60] Pavinato L, Delle Vedove A, Carli D, Ferrero M, Carestiato S, Howe JL, et al. CAPRIN1 haploinsufficiency causes a neurodevelopmental disorder with language impairment, ADHD and ASD. Brain. 2023;146:534-48.
[61] Solomon S, Xu Y, Wang B, David MD, Schubert P, Kennedy D, et al. Distinct structural features of caprin-1 mediate its interaction with G3BP-1 and its induction of phosphorylation of eukaryotic translation initiation factor 2alpha, entry to cytoplasmic stress granules, and selective interaction with a subset of mRNAs. Mol Cell Biol. 2007;27:2324-42.
[62] Shiina N, Yamaguchi K, Tokunaga M. RNG105 deficiency impairs the dendritic localization of mRNAs for Na+/K+ ATPase subunit isoforms and leads to the degeneration of neuronal networks. J Neurosci. 2010;30:12816-30.
[63] Martin S, Zekri L, Metz A, Maurice T, Chebli K, Vignes M, et al. Deficiency of G3BP1, the stress granules assembly factor, results in abnormal synaptic plasticity and calcium homeostasis in neurons. J Neurochem. 2013;125:175-84.
[64] Wolozin B, Ivanov P. Stress granules and neurodegeneration. Nat Rev Neurosci. 2019;20:649-66.
[65] Nixon RA. Amyloid precursor protein and endosomal-lysosomal dysfunction in Alzheimer's disease: inseparable partners in a multifactorial disease. FASEB J. 2017;31:2729-43.
[66] Drummond E, Wisniewski T. Alzheimer's disease: experimental models and reality. Acta Neuropathol. 2017;133:155-75.
[67] Strovel J, Sittampalam S, Coussens NP, Hughes M, Inglese J, Kurtz A, et al. Early Drug Discovery and Development Guidelines: For Academic Researchers, Collaborators, and Start-up Companies. In: Markossian S, Grossman A, Brimacombe K, Arkin M, Auld D, Austin C, et al., editors. Assay Guidance Manual. Bethesda (MD)2004.

(A)

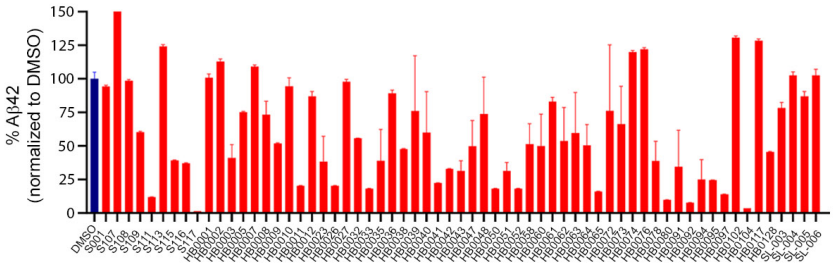

(C)

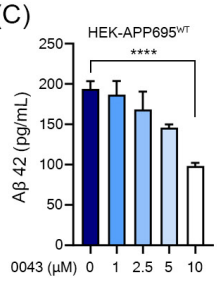

(B)

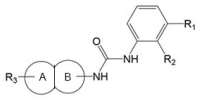

Compounds	Rings A+B	R1	R2	R3	HEK-APP695WT Aβ42 decrease (% of DMSO)	iPSC-N Aβ42 decrease (% of DMSO)	iPSC-N Viability (IC_{50} μM)
0047		≡N			50.1	60.7	2.9
0043		≡N			68.6	55.6	49.8
0078		≡N	F	Cl	61.1	39.6	6.4
0048		≡N			26.2	35.3	62.9
0062		≡N			46.3	34.8	50.2
0035		≡N		CH3	61.0	31.0	13.2
0063		Cl			40.3	16.6	

(D)

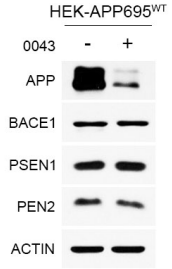

(E)

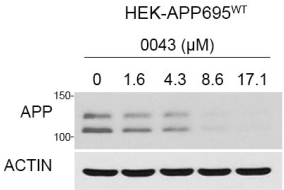

(F)

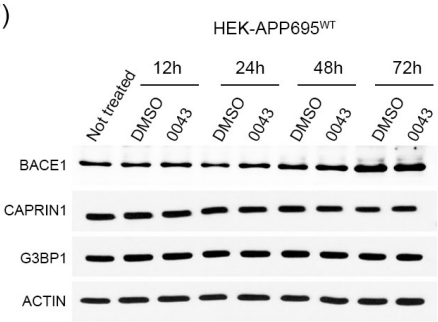

(G)

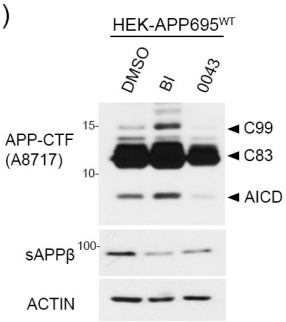

(H)

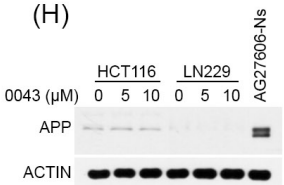

Figure 1 Screening of CAPRIN1-targeted molecules that reduce Aβ42 and APP. **(**A) The Aβ42 levels (% of compound vs DMSO) in culture media of HEK-APP695^{WT} treated with each molecule (10 μM) for 4 days (means ± SD, n=3). (B) The chemical scaffold (*top*) and structures of the compounds and the effects on Aβ42 reduction and cell viability of HEK-APP695^{WT} and AD iPSC AG27606-Ns. (C) The Aβ42 levels in culture media of HEK-APP695^{WT} treated with various doses of 0043 (means ± SD, n=3). (D) Western blots of the levels of the proteins as indicated (*left*) in HEK-APP695^{WT} treated with 0043 (10 μM) for 3 days. (E) Western blots of the levels of the indicated proteins in HEK-APP695^{WT} treated with various doses of 0043 for 3 days. (F) Western blots of the levels of the proteins in HEK-APP695^{WT} treated with 0043 or DMSO for different hours as indicated (*top*). (G) Western blots of the indicated proteins in HEK-APP695^{WT} treated with 0043 as determined by APP-CTFs (A8717) and sAPP-beta antibodies. (H) Western blots of APP levels in human colon cancer HCT116 and glioblastoma LN229 cells treated with 0043 at 10 μM for 3 days. AD iPSC AG27606-Ns were used as a neuronal control.

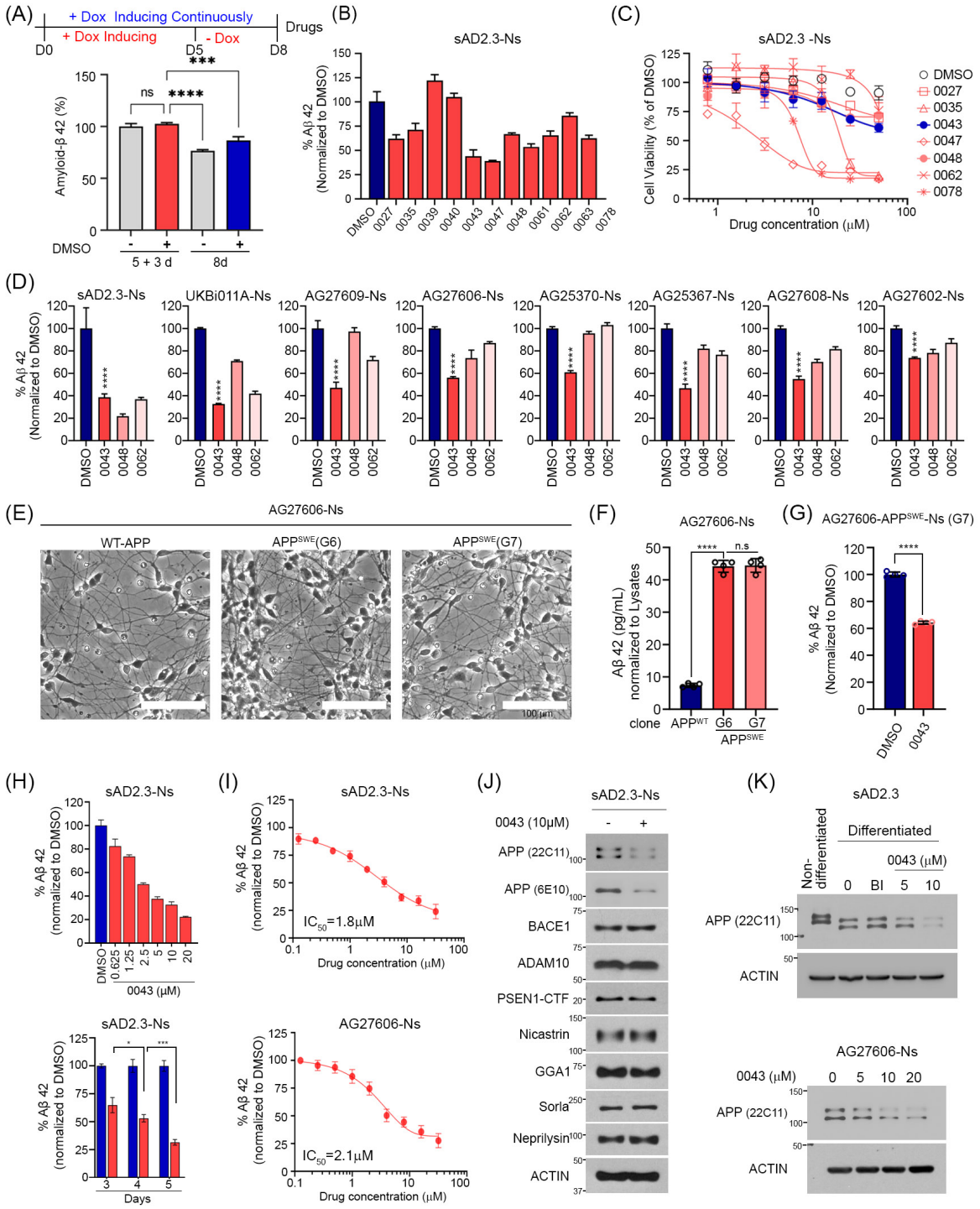
(A)
+ Dox Inducing Continuously
+ Dox Inducing
- Dox
Drugs
D0
D5
D8
Amyloid-β 42 (%)
ns
****
***
DMSO
5 + 3 d
8d
(B)
sAD2.3-Ns
% Aβ 42 (Normalized to DMSO)
DMSO
0027
0035
0039
0040
0043
0047
0048
0061
0062
0063
0078
(C)
sAD2.3 -Ns
Cell Viability (% of DMSO)
Drug concentration (μM)
DMSO
0027
0035
0043
0047
0048
0062
0078
(D)
sAD2.3-Ns
UKBi011A-Ns
AG27609-Ns
AG27606-Ns
AG25370-Ns
AG25367-Ns
AG27608-Ns
AG27602-Ns
% Aβ 42 (Normalized to DMSO)
DMSO
0043
0048
0062
(E)
AG27606-Ns
WT-APP
APPSWE(G6)
APPSWE(G7)
100 μm
(F)
AG27606-Ns
Aβ 42 (pg/mL) normalized to Lysates
n.s
clone
APPWT
G6
G7
APPSWE
(G)
AG27606-APPSWE-Ns (G7)
% Aβ 42 (Normalized to DMSO)
DMSO
0043
(H)
sAD2.3-Ns
% Aβ 42 (normalized to DMSO)
DMSO
0.625
1.25
2.5
5
10
20
0043 (μM)
sAD2.3-Ns
Days
(I)
sAD2.3-Ns
% Aβ 42 (normalized to DMSO)
IC50=1.8μM
Drug concentration (μM)
AG27606-Ns
IC50=2.1μM
Drug concentration (μM)
(J)
sAD2.3-Ns
0043 (10μM)
APP (22C11)
APP (6E10)
BACE1
ADAM10
PSEN1-CTF
Nicastrin
GGA1
Sorla
Neprilysin
ACTIN
(K)
sAD2.3
Non-differentiated
Differentiated
0043 (μM)
0
BI
5
10
APP (22C11)
ACTIN
AG27606-Ns
0043 (μM)
0
5
10
20
APP (22C11)
ACTIN

Figure 2 The compound 0043 reduces Aβ42 and APP in AD-iPSC-Ns. (A) ELISA of Aβ42 levels in culture media of iPSC-Ns under two Dox inducing protocols (means ± SD; ***$p<0.001$, ****$p<0.0001$, ns=non-significance). (B) ELISA of Aβ42 in culture media of sAD2.3-Ns treated with each compound (10 μM) for 4 days. (C) Cell viability assay of sAD2.3-Ns treated with a series of doses of indicated compounds for 4 days (means ± SD; n=3). (D) ELISA of Aβ42 levels in culture media of each of the panel of eight iPSC-Ns treated with indicated compounds (10 μM) for 4 days (means ± SD; ****$p<0.0001$; n=4). (E) Contrast microscopes of APP^{SWE} mutant AG27606-Ns (the scale = 100 μm). (F) ELISA of Aβ42 levels in the cultures of APP^{SWE} mutant and APP^{WT} AG27606-Ns (means ± SD; ****$p<0.0001$; n=4). (G) ELISA of Aβ42 levels in the cultures of APP^{SWE} AG27606-Ns treated with 0043 (10 μM) for 4 days (means ± SD; ****$p<0.0001$; n=4). (H) ELISA of Aβ42 in the cultures of sAD2.3-Ns treated with a series of doses of 0043 (*top*) for 5 days or one dose of 0043 (10 μM) for indicated days (*bottom*; means ± SD; *$p<0.05$; ***$p<0.001$; n=3). (I) ELISA of Aβ42 in the cultures of sAD2.3-Ns and AG27606-Ns treated with a series of dilutions of 0043 for 5 days with the IC_{50} values indicated. (J) Western blots of indicated proteins in sAD2.3-Ns treated with 0043 (10 μM) or DMSO for 3 days. (K) Western blots of sAD2.3-Ns and AG27606-Ns with the indicated doses of 0043 for 3 days.

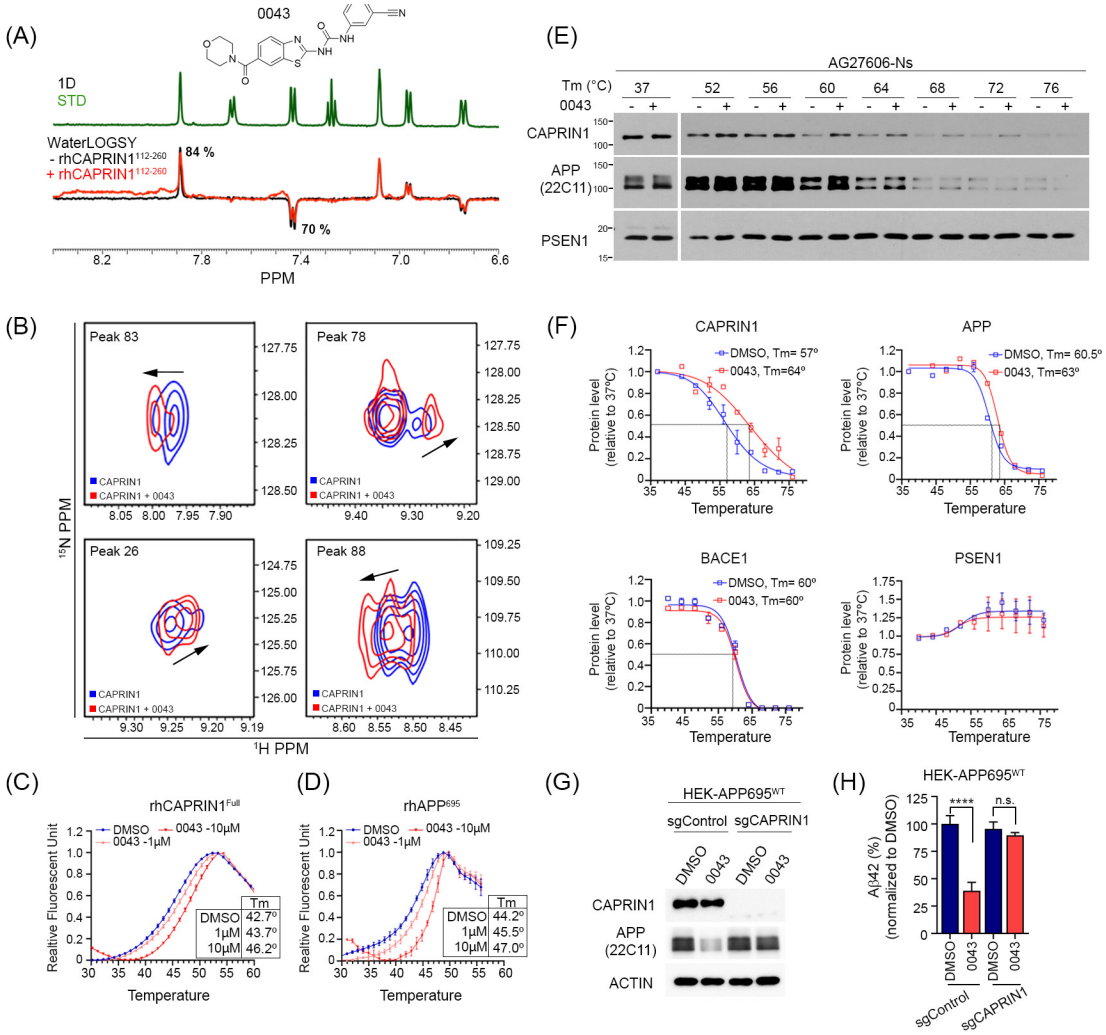
(A)
0043
1D
STD
WaterLOGSY
- rhCAPRIN1112-260
+ rhCAPRIN1112-260
84 %
70 %
PPM
(B)
Peak 83
Peak 78
Peak 26
Peak 88
CAPRIN1
CAPRIN1 + 0043
15N PPM
1H PPM
(C)
rhCAPRIN1Full
DMSO
0043 -10μM
0043 -1μM
Tm
DMSO 42.7°
1μM 43.7°
10μM 46.2°
Realtive Fluorescent Unit
Temperature
(D)
rhAPP695
DMSO 44.2°
1μM 45.5°
10μM 47.0°
(E)
AG27606-Ns
Tm (°C)
0043
CAPRIN1
APP (22C11)
PSEN1
(F)
CAPRIN1
DMSO, Tm= 57°
0043, Tm=64°
APP
DMSO, Tm= 60.5°
0043, Tm=63°
BACE1
DMSO, Tm= 60°
0043, Tm=60°
PSEN1
Protein level (relative to 37°C)
Temperature
(G)
HEK-APP695WT
sgControl
sgCAPRIN1
DMSO
0043
CAPRIN1
APP (22C11)
ACTIN
(H)
HEK-APP695WT
Aβ42 (%) (normalized to DMSO)
****
n.s.
sgControl
sgCAPRIN1

Figure 3 The compound 0043 directly binds CAPRIN1 and APP. (A) NMR spectrum of 200 μM 0043 in green (*top*) and 1D-WaterLOGSY spectra recorded of 200 μM 0043 where red and black spectrum corresponds to 0043 in the presence and absence of 20 μM CAPRIN1, respectively. (B) Representative backbone amide peaks in the ^{1}H-^{15}N-HSQC spectrum of CAPRIN1 alone (blue) and in the presence of 0043 (red). The direction of peak shifts is shown by the black arrows. (C,D) Thermofluor shift assay of rhCAPRIN1^{Full} (C) and rhAPP^{Full} (D) in the presence of indicated doses of 0043. (E,F) Western blots of CETSA (E) and levels of indicated proteins at a temperature point relative to that 37°C (F) in AG27606-Ns in the absence and presence of 0043 (10 μM) with increased temperature. (G) Western blots for APP and CAPRIN1 in sgCAPRIN1 and sgRNA control HEK-APP695^{WT} clones treated or untreated with 0043 (10μM). (H). ELISA of Aβ42 levels in culture media of sgCAPRIN1 and sgControl HEK-APP695^{WT} clones after treated with 0043 (10 μM) for 3 days (means ± SD; ****$P < 0.0001$, ns: non-significance, n=3).

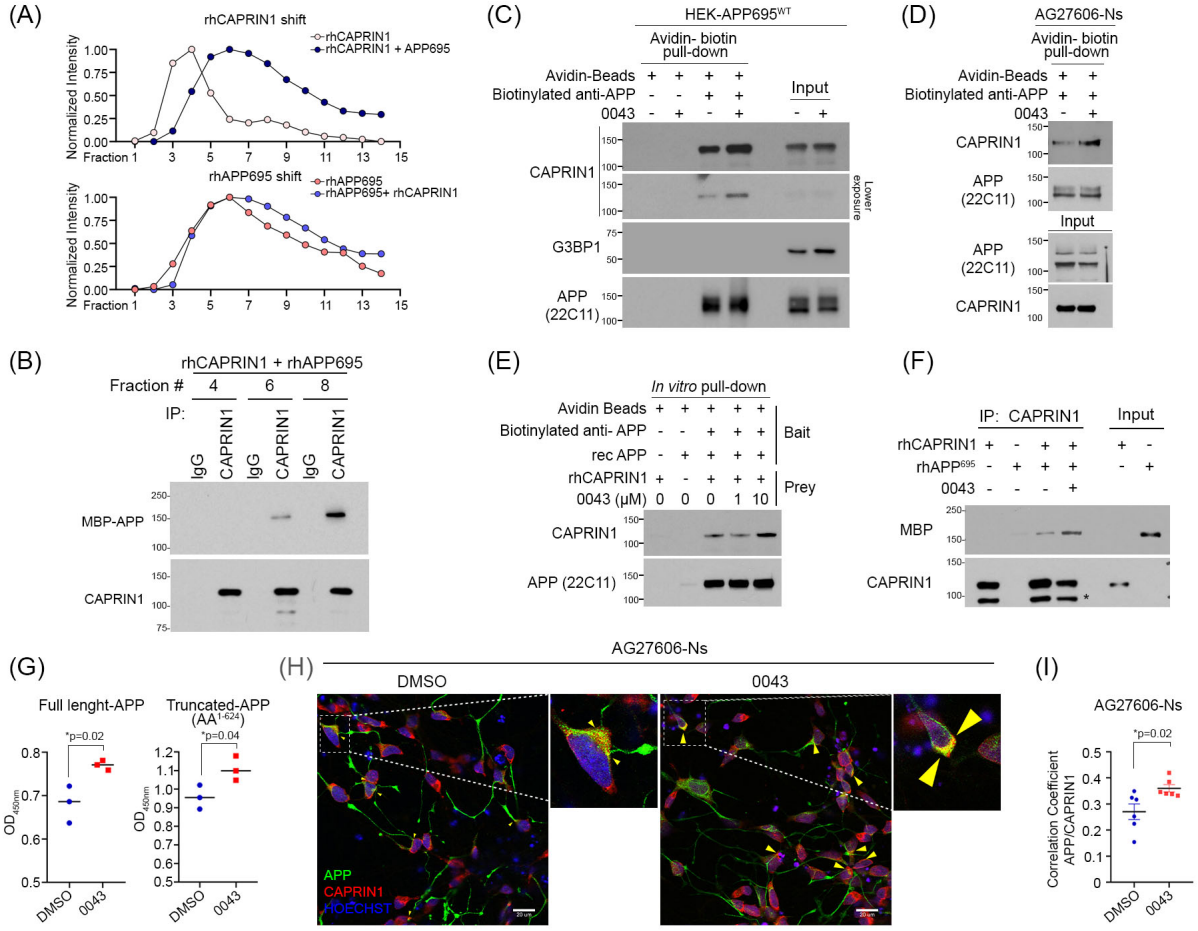
(A)
rhCAPRIN1 shift
rhCAPRIN1
rhCAPRIN1 + APP695
Normalized Intensity
Fraction
rhAPP695 shift
rhAPP695
rhAPP695+ rhCAPRIN1
(B)
rhCAPRIN1 + rhAPP695
Fraction #
IP:
IgG
CAPRIN1
MBP-APP
CAPRIN1
(C)
HEK-APP695WT
Avidin- biotin pull-down
Avidin-Beads
Biotinylated anti-APP
0043
Input
CAPRIN1
lower exposure
G3BP1
APP (22C11)
(D)
AG27606-Ns
Avidin- biotin pull-down
Avidin-Beads
Biotinylated anti-APP
0043
CAPRIN1
APP (22C11)
Input
APP (22C11)
CAPRIN1
(E)
In vitro pull-down
Avidin Beads
Biotinylated anti- APP
rec APP
rhCAPRIN1
0043 (μM)
Bait
Prey
CAPRIN1
APP (22C11)
(F)
IP: CAPRIN1
Input
rhCAPRIN1
rhAPP695
0043
MBP
CAPRIN1
(G)
Full lenght-APP
Truncated-APP (AA1-624)
*p=0.02
*p=0.04
OD450nm
DMSO
0043
(H)
AG27606-Ns
DMSO
0043
APP
CAPRIN1
HOECHST
(I)
AG27606-Ns
*p=0.02
Correlation Coefficient APP/CAPRIN1
DMSO
0043

Figure 4 The 0043 binding of CAPRIN1 and APP enhances the protein-protein interaction. (A) The fractional distribution of individual and mixed rhCAPRIN1 and rhAPP695 across glycerol gradient (the protein levels were quantified from Supplementary Figure 4A by Image J program). (B) Western blots by anti-MBP antibody of the immunoprecipitation or by CAPRIN1 antibody of selected fractions as indicated with black arrows in the glycerol gradient as presented in Supplementary Figure 4A. (C,D) Western blots of APP-biotin-Streptavidin pull-down of HEK-APP695^{WT} clones (C) and AG27606-Ns (D) after treated with 0043 (10 μM) for APP interaction with CAPRIN1 or G3BP1. Whole cell lysate (WCL) was used as the loading control. (E) Western blots of avidin-APP-biotin antibodies pull-downs of rhAPP^{Full} and rhCAPRIN1^{Full} in the presence of 0043 at indicated concentrations. (F) Western blots of anti-CAPRIN1 antibody/agarose G bead pull-downs of rhCAPRIN1^{Full} and rhAPP^{Full}-MBP in the presence or absence of 0043. (G) Direct ELISA of CAPRIN1 interacted with rhAPP^{Full} or rhAPP^{Truncated} in the absence or presence of 0043. (H,I) Confocal microscopes (h) of AG27606-Ns after treated with 0043 for 24 hours and stained as indicated (green, APP antibodies; red: CAPRIN1 antibodies; and blue: HOECHST (scale bar = 20 μm) and the correlation coefficient values (i) of APP and CAPRIN1 analyzed by using the Image J program.

(A)

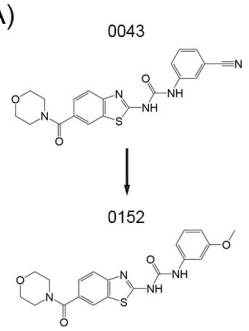

(B)

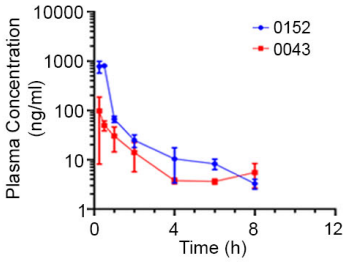

(C)

Compounds	0043	0152
Dose (mg/kg) Oral/IV	10	10
Oral Formulation	NMP/PG/TPGS/ Captisol	NMP/PG/Solutol HS-15/ Captisol
PO C_0/C_{max} (ng/ml)	97	804
PO AUC_{last} (h*ng/ml)	107	624
$T_{1/2}$ (h) Oral	1.6	2.4
Vd_{ss}	0.8	1.3
Oral Bioavaibility (%)	5	30

(D)

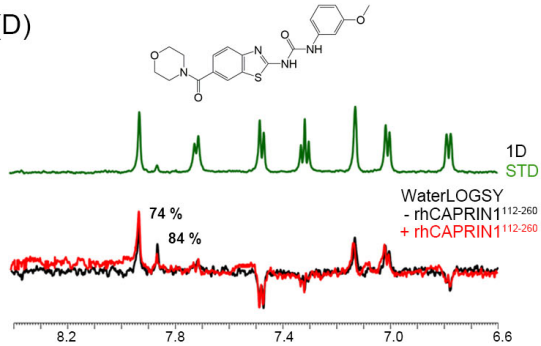

(E)

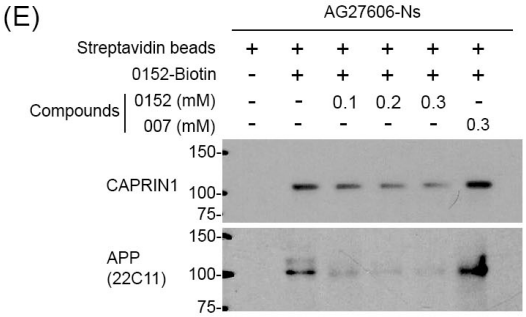

(F)

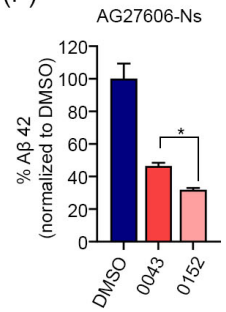

(G)

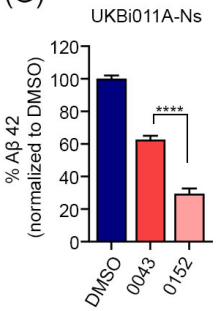

(H)

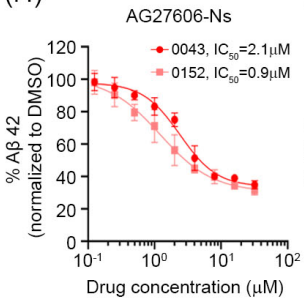

(I)

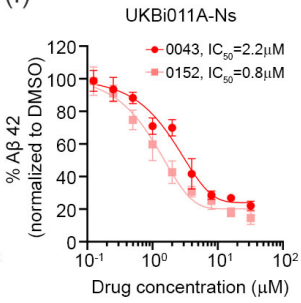

(J)

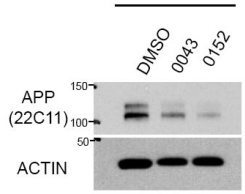

(K)

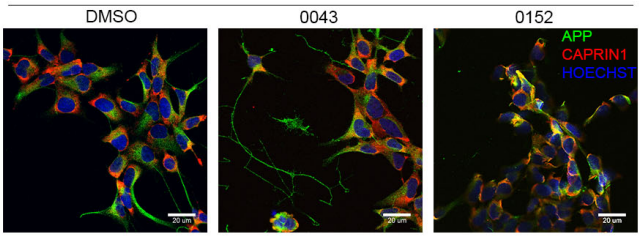

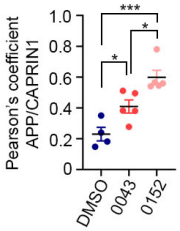

Figure 5 Identification of the lead 0152 from chemical modification of the hit 0043. (A) The chemical structures of the hit compound 0043 and its derivative lead 0152. (B) The PK assessment of 0043 and 0152 by analyzing mouse plasma at different time points after oral administration of the compounds (n= 3). (C) The PK values of 0043 and 0152 determined by analyzing the compounds in mouse plasma samples after administrated orally in indicated doses and solution formulations. (D) NMR spectrum of 0152 in green (*top*) and 1D-WaterLOGSY spectra recorded of 0152 where red and black spectrum corresponds to 0152 in the presence or absence of 20 μM CAPRIN1. (E) Western blots of biotin-0152/streptavidin-coated bead-pull downs of AG27606-Ns lysates in the presence of various doses of 0152 and HB007. (F,G) ELISA of Aβ42 in culture media of AG27606-Ns (f) and UKBi011A-Ns (g) after treated with 0043 and 0152 (10 μM) for 4 days (means ± SD; **$p<0.01$, ****$p<0.0001$; n=4). (H,I) ELISA of Aβ42 in culture media of AG27606-Ns (H) and UKBi011A-Ns (I) after treated with various doses of 0043 and 0152 for 5 days with the IC_{50} values calculated. (J) Western blot of APP in AG27606-Ns after treated with 0043 (10 μM) and 0152 (10 μM) for 5 days. (K) Confocal microscopes (*left*) of AG27606-Ns after treated with 0043 (10 μM) and 0152 (10 μM) for 24 hours and stained as indicated (green, APP antibodies; red: CAPRIN1 antibodies; and blue: HOECHST (scale bar = 20 μm) and the correlation coefficient values (*right*) of APP and CAPRIN1 analyzed using the Image J program (means ± SD; *$p<0.05$, ***$p<0.001$).

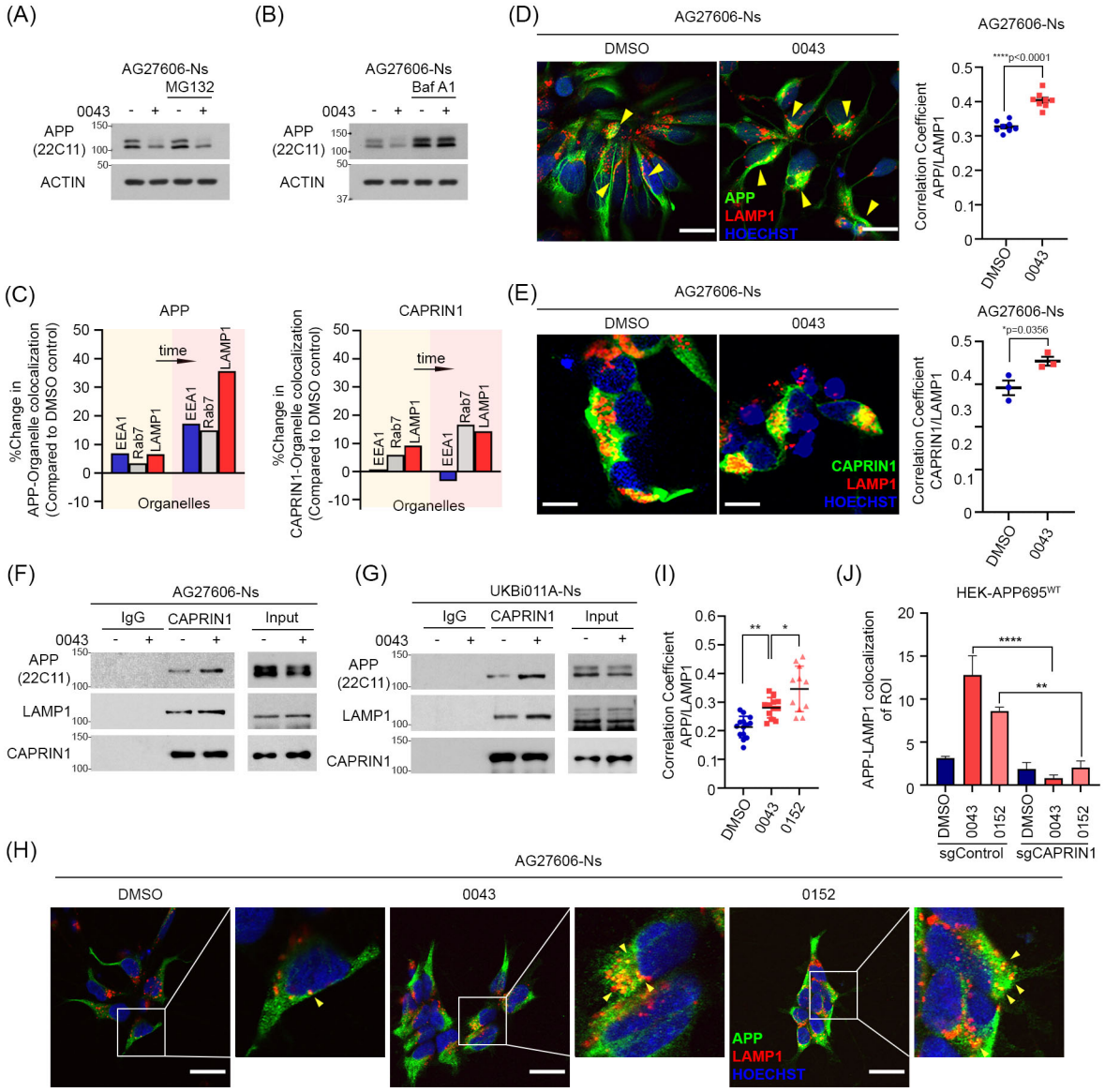
(A)
AG27606-Ns
MG132
0043 - + - +
APP (22C11)
ACTIN
(B)
AG27606-Ns
Baf A1
0043 - + - +
APP (22C11)
ACTIN
(C)
APP
%Change in APP-Organelle colocalization (Compared to DMSO control)
time
EEA1
Rab7
LAMP1
Organelles
CAPRIN1
%Change in CAPRIN1-Organelle colocalization (Compared to DMSO control)
(D)
AG27606-Ns
DMSO
0043
APP
LAMP1
HOECHST
Correlation Coefficient APP/LAMP1
****p<0.0001
(E)
AG27606-Ns
DMSO
0043
CAPRIN1
LAMP1
HOECHST
Correlation Coefficient CAPRIN1/LAMP1
*p=0.0356
(F)
AG27606-Ns
IgG
CAPRIN1
Input
0043
APP (22C11)
LAMP1
CAPRIN1
(G)
UKBi011A-Ns
IgG
CAPRIN1
Input
0043
APP (22C11)
LAMP1
CAPRIN1
(I)
Correlation Coefficient APP/LAMP1
DMSO
0043
0152
(J)
HEK-APP695WT
APP-LAMP1 colocalization of ROI
DMSO
0043
0152
sgControl
sgCAPRIN1

(H)

AG27606-Ns
DMSO
0043
0152
APP
LAMP1
HOECHST

Figure 6 The degraders induce APP lysosomal degradation in iPSC neurons. (A,B) Western blots of AG27606-Ns after pretreated with MG132 (5 μM) or Bafilomycin A1 (20 nM) for 30 minutes and then with 0043 (10 μM) for 24 hours. (C)The organelle subcellular distributions of APP (*left*) and CAPRIN1 (*right*) as colocalized with indicated organelle markers in AG27606-Ns after 3 hours and 7 hours of 0043 treatment (10 μM). (D,E) Confocal microscopes (*left*) and correlation coefficient values of APP-LAMP1 (d) and CAPRIN1-LAMP1 (e) in AG27606-Ns after treated with 0043 for 24 hours and stained as indicated (APP/CAPRIN1; green, LAMP1; red, HOECHST; blue, scale bar = 20 μm, yellow arrow: colocalization). (F,G) Immunoprecipitation and western blots of APP, LAMP1 and CAPRIN1 in AG27606-Ns (f) and UKBi011A-Ns (g) after treated with 0043 for 24 hours. IgG was used as a negative control. (H,I) Confocal microscopes AG27606-Ns (H) after treated with indicated compounds (10 μM) for 24 hours and stained as indicated (APP; green, LAMP1; red, HOECHST; blue, scale bar = 20 μm). The correlation coefficient value of APP-LAMP1 (I) was determined by Image J program (means ± SD; *$p<0.05$, **$p<0.01$). (J) The colocalization of APP-LAMP1 in sgControl and sgCAPRIN1 HEK-APP695^{WT} clones after treated with indicated compounds (10 μM) for 1 day and stained with LAMP1 and APP as presented in Supplementary Figure 6J (means ± SD, **$p<0.01$, ****$p<0.0001$).

(A)

	AD #1	AD #2	AD #3	AD #4	non-AD
Age, Sex	70, F	64, F	67, M	67, F	64, F
Path Diagnose	AD	AD	AD	AD	No
Neuron	+++	+++	+++	+++	+++
CAPRIN1	+++	+++	+++	+++	+++
Astrocytes	-	-	-	-	-
Oligodendroglia	-	-	-	-	-
Endothelial cells	-	-	-	-	-

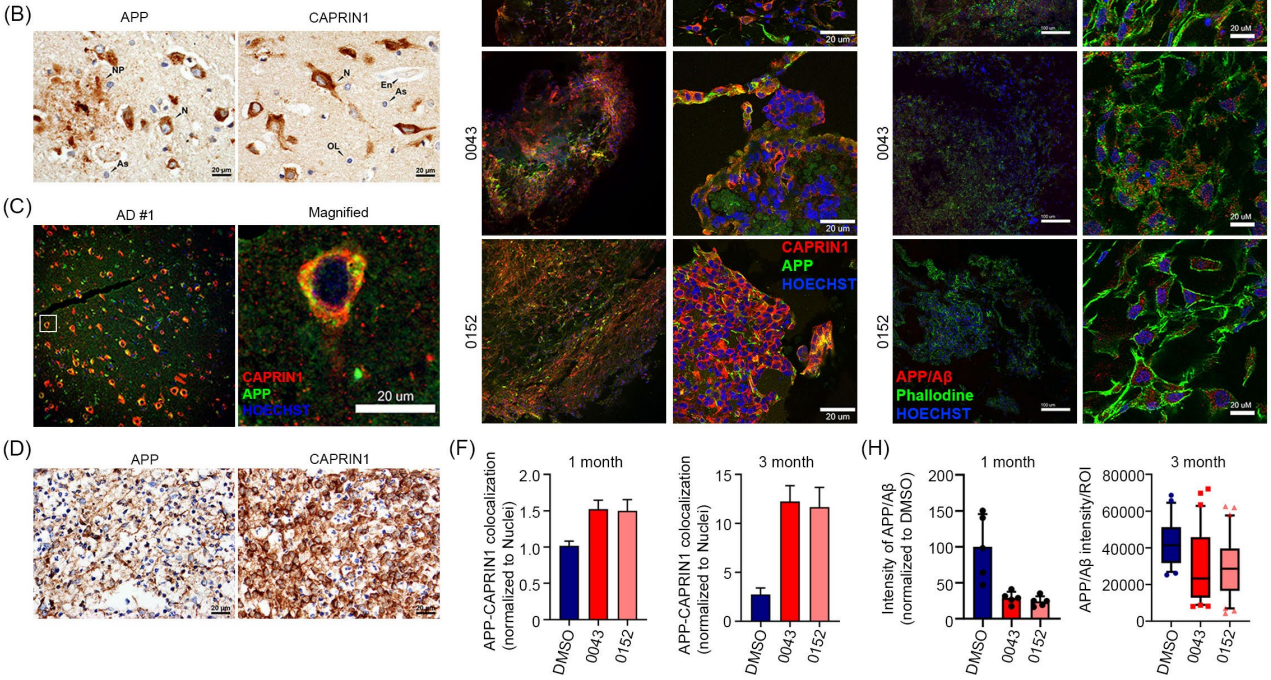

Figure 7 APP degraders reduce Aβ42 levels in AD iPSC-derived brain organoids. (A) Semi-quantification of CAPRIN1 expression as determined by IHC in autopsy brains of AD and non-AD individuals with related clinical information. (B) IHC of APP and CAPRIN1 in cerebral cortex of a representative AD brain (Scale bar = 20 μm; N: Neurons, As: Astrocytes, En: Endothelial cells, OL: Oligodendroglia, NP: Neuritic Plague). (C) Immunofluorescence confocal microscopes of a representative AD brain stained with CAPRIN1 and APP antibodies (green: APP, red: CAPRIN1; blue: HOECHST, scale bar = 20 μm). (D) IHC of APP CAPRIN1 in AG27606-3D organoids (Scale bar = 20 μm). (E,F) Immunofluorescence confocal microscopes (E) and colocalization of APP and CAPRIN1 (F) in AG27606-3D organoids after treated with 0043 and 0152 for 1 month or 3 months and stained as indicated (green: APP, red: CAPRIN1, scale bar = 20 μm). (G,H) Immunofluorescence confocal microscopes (G) and intensities of APP/Aβ as analyzed by Image J (H) in AG27606-3D organoids after treated with 0043 and 0152 for 1 month or 3 months. Phalloidine was used for actin filaments (scale bar = 20 μm).